Research
A SCIENCE PARTNER JOURNAL

RESEARCH ARTICLE

Progressive Deactivation of Hydroxylases Controls Hypoxia-Inducible Factor-1α-Coordinated Cellular Adaptation to Graded Hypoxia

Ping Wang[1,2], Xiao-Peng Zhang[1,3*], Feng Liu[3,4*], and Wei Wang[3,4*]

[1]Kuang Yaming Honors School, Nanjing University, Nanjing 210023, China. [2]Key Laboratory of High Performance Scientific Computation, School of Science, Xihua University, Chengdu 610039, China. [3]Institute of Brain Sciences, Nanjing University, Nanjing 210093, China. [4]National Laboratory of Solid State Microstructures and Department of Physics, Nanjing University, Nanjing 210093, China.

*Address correspondence to: zhangxp@nju.edu.cn (X.-P.Z.); fliu@nju.edu.cn (F.L.); wangwei@nju.edu.cn (W.W.)

Citation: Wang P, Zhang X-P, Liu F, Wang W. Progressive Deactivation of Hydroxylases Controls Hypoxia-Inducible Factor-1α-Coordinated Cellular Adaptation to Graded Hypoxia. *Research* 2025;8:Article 0651. https://doi.org/10.34133/research.0651

Submitted 20 December 2024
Revised 26 February 2025
Accepted 8 March 2025
Published 1 April 2025

Graded hypoxia is a common microenvironment in malignant solid tumors. As a central regulator in the hypoxic response, hypoxia-inducible factor-1 (HIF-1) can induce multiple cellular processes including glycolysis, angiogenesis, and necroptosis. How cells exploit the HIF-1 pathway to coordinate different processes to survive hypoxia remains unclear. We developed an integrated model of the HIF-1α network to elucidate the mechanism of cellular adaptation to hypoxia. By numerical simulations and bifurcation analysis, we found that HIF-1α is progressively activated with worsening hypoxia due to the sequential deactivation of the hydroxylases prolyl hydroxylase domain enzymes and factor inhibiting HIF (FIH). Bistable switches control the activation and deactivation processes. As a result, glycolysis, immunosuppression, angiogenesis, and necroptosis are orderly elicited in aggravating hypoxia. To avoid the excessive accumulation of lactic acid during glycolysis, HIF-1α induces monocarboxylate transporter and carbonic anhydrase 9 sequentially to export intracellular hydrogen ions, facilitating tumor cell survival. HIF-1α-induced miR-182 facilitates vascular endothelial growth factor production to promote angiogenesis under moderate hypoxia. The imbalance between accumulation and removal of lactic acid in severe hypoxia may result in acidosis and induce cell necroptosis. In addition, the deactivation of FIH results in the destabilization of HIF-1α in anoxia. Collectively, HIF-1α orchestrates the adaptation of tumor cells to hypoxia by selectively inducing its targets according to the severity of hypoxia. Our work may provide clues for tumor therapy by targeting the HIF-1 pathway.

Introduction

Hypoxia is a hallmark of the tumor microenvironment. In advanced solid tumors, malignant proliferation of tumor cells progressively distances themselves from blood vessels, thereby exacerbating hypoxia [1]. In the bone marrow, the oxygen partial pressure along individual blood vessels decreases gradually, indicating the presence of a hypoxic gradient [2]. Histological analysis of tissues from different cancer patients exhibits some typical properties including malignant proliferation, central necroptosis, and peripheral microvascular proliferation [3–5]. These heterogeneous morphological features may result from differential adaptive responses of tumor cells to graded hypoxia, as demonstrated in 3-dimensional tumor spheroid models [6]. However, the molecular mechanisms underlying tumor cell adaptation to varying levels of hypoxia remain less understood.

Hypoxia-inducible factor-1 (HIF-1), composed of oxygen-regulated HIF-1α and constitutively expressed HIF-1β, plays a key role in the cellular response to hypoxia [7,8]. In hypoxia, HIF-1α accumulates in cells and acquires transcriptional activity [9]. As a transcription factor, it can induce a series of target genes to mediate various cellular processes including glycolysis, angiogenesis, drug resistance, necroptosis, and cell migration [10]. It is a substantial challenge to understand how tumor cells exploit HIF-1α to orchestrate different responses to survive hypoxia.

The stability and transcriptional activity of HIF-1α are modulated by hydroxylases PHDs (prolyl hydroxylase domain enzymes) and FIH (factor inhibiting HIF). In normoxia, PHDs utilize oxygen and 2-oxoglutarate as co-substrates to hydroxylate HIF-1α on P402/P564 in the N-terminal transcriptional domain, leading to its degradation by von Hippel-Lindau (VHL) [11–13]. The transcriptional activity of HIF-1α is suppressed by FIH, which hydroxylates it on Asn803 in the C-terminal transcriptional domain (C-TAD) and prevents it from binding to transcriptional cofactors p300/CBP [14]. The independent regulation of stability and activity of HIF-1α by PHDs and FIH highlights their nonredundant roles in modulating HIF-1α function [15].

Under hypoxia, PHDs and FIH deactivate at different oxygen concentrations, leading to the progressive activation of HIF-1α [16]. It remains to be elucidated how PHDs and FIH coordinate to control HIF-1α activity and its selective induction of targets under hypoxia.

Increasing experimental evidence underscores the role of microRNAs (miRNAs) in regulating HIF-1α signaling [17,18]. In particular, miR-155, miR-210, and miR-182 are induced by HIF-1α and, in turn, regulate it via PHDs and FIH [19–22]. Among them, HIF-1α induces miR-182 to reduce the expression of PHD-2 and FIH, thereby amplifying its activation by positive feedback loops. On the other hand, HIF-1α up-regulates PHD-2 to repress its own activation, forming a negative feedback loop. Considering these feedback loops may add another layer of complexity to HIF-1α signaling. It is intriguing to clarify how feedback loops synergize to modulate the response of HIF-1α to hypoxia.

Tumor cells exploit HIF-1α signaling to adapt to hypoxia through multiple strategies. A remarkable adaptive response induced by HIF-1α is to increase glycolysis, compensating for reduced oxidative phosphorylation in energy metabolism [23]. HIF-1α promotes the shift to anaerobic metabolism by inducing various glycolytic enzymes, while decreasing mitochondrial oxygen consumption by up-regulating pyruvate dehydrogenase kinase 1 (PDK1) to attenuate the tricarboxylic acid (TCA) cycle [10,24–26]. However, this strategy alone would bring about a serious threat to cell survival. Lactic acid is a typical by-product of glycolysis. Excessive accumulation of intracellular acid leads to acidosis, triggering cell necroptosis in a BNIP3-dependent manner [27,28]. In addition, HIF-1α can alleviate hypoxic dilemmas by promoting immunosuppression [29] and angiogenesis [30]. It is still challenging to unravel the mechanism by which hypoxic cells choose among different outcomes based on the severity of hypoxia.

To relieve the survival stress caused by the accumulation of lactic acid, HIF-1 activates several proton exchangers and ion channels to produce an alkaline intracellular environment. Monocarboxylate transporter (MCT) and carbonic anhydrase 9 (CA9) are 2 representative targets of HIF-1, with the former responsible for exporting hydrogen ions and the latter contributing to intracellular H^+ neutralization [27]. Notably, this acidic extracellular environment confers a growth advantage to cancer by inducing cell growth [31], blunting the immune system [32] and promoting epithelial–mesenchymal transition (EMT) involved in metastasis [33]. That is, HIF-1 acts as a potent regulator of the redistribution of intracellular and extracellular acids. It remains unclear how HIF-1 balances adenosine triphosphate (ATP) reduction and excessive lactic acid during the formation of an acidic microenvironment.

A series of models has been developed to reveal the mechanism underlying the modulation of HIF-1α dynamics. As the oxygen level decreases, HIF-1α appears to have a switch-like behavior; i.e., it remains low at wide oxygen levels and increases exponentially to high concentrations at narrow oxygen levels [34]. Qutub et al. [35] demonstrated that saturated substrates required for PHD-2 catalysis contribute to switch-like reactions, and the presence of any molecular unsaturation in these substrates results in a progressive response of HIF-1α to hypoxia. Bagnall et al. [36] proposed that the adaptive dynamics of HIF-1α in response to hypoxia is controlled by the HIF-1α-PHD negative feedback loop. Nguyen et al. [37] found that the remarkable decrease in HIF-1α levels in severe hypoxia should be associated with the destabilization of HIF-1α without the protection of FIH-mediated hydroxylation. Although most models have focused on the mechanism underlying the generation of HIF-1α dynamics, a comprehensive model of how different cellular processes are regulated by the HIF-1α dynamics is still lacking.

Here, we developed a network model to explore how HIF-1α mediates the adaptive response of tumor cells to hypoxia. We probed how cellular outcome was associated with network dynamics, the regulation of HIF-1α activity by PHD-2 and FIH, the role of miR-182 in modulating HIF activity and angiogenesis, and how the accumulation of lactic acid and its intracellular/extracellular distribution were modulated. We found that the coupled feedback loops involving HIF-1α, miR-182, FIH, and PHD-2 determine the selective induction of HIF-1 targets, linking the circuit regulation of HIF-1α with its physiological functions.

Results

Network model

We developed an integrated model of the HIF-1α network and explored the network dynamics and cellular adaptive response under hypoxia (Fig. 1). PHD-2, FIH, and miR-182 are involved in the modulation of the stability and activity of HIF-1α under hypoxia. phosphofructokinase liver type (PFKL), A2B, vascular endothelial growth factor (VEGF), and BNIP3 are 4 effectors of HIF-1α, whose high expressions and/or activation represent the initiation of glycolysis, immunosuppression, angiogenesis, and necroptosis, respectively. The details of model construction are presented as follows.

Regulation of HIF-1α by PHD-2 and FIH

The prolyl hydroxylase family mainly consists of PHD-1, PHD-2, and PHD-3. PHD-1 and PHD-2 are localized in the nucleus and cytoplasm, respectively, while PHD-3 is present in both compartments [38]. Since PHD-1 and PHD-3 preferentially target HIF-2α [39] and PHD-2 has a remarkable advantage over PHD-1/PHD-3 in hydroxylating HIF-1α [40], we considered the regulation of HIF-1α by PHD-2 alone. FIH promotes the hydroxylation of HIF-1α on Asn803, inhibiting its transcriptional activity while repressing its PHD-independent degradation [37].

Two forms of HIF-1α were considered according to their hydroxylation status associated with their activity. Considering that C-TAD-truncated HIF-1α retains one-third of its full transcriptional activity [41], it was assumed that HIF-1α-aOH is the partially activated form that is hydroxylated on Asn803 in C-TAD alone. The entirely dehydroxylated HIF-1α was considered the fully activated form. Moreover, PHD-2 and FIH were divided into inactive (PHD-2 and FIH) and active ($PHD\text{-}2^*$ and FIH^*) forms. The activation of the 2 hydroxylases depends on oxygen levels. Based on experimental results, we assumed that the threshold of oxygen levels for FIH activation (j_{O2FIH}) is much lower than that for PHD-2 (j_{O2PHD}) since PHD-2 is deactivated before FIH with worsening hypoxia [16] (see Eqs. 5 and 8 in the Supplementary Materials). The total amounts of PHD-2 and FIH are represented by $PHD\text{-}2_T$ and FIH_T, respectively.

Both HIF-1α-aOH and HIF-1α were assumed to be degraded in $PHD\text{-}2^*$-dependent and -independent ways (see Eqs. 1 and 2 in the Supplementary Materials). For simplicity, the role of pVHL is implicated in PHD-2-dependent degradation of HIF-1α in which pVHL targets the hydroxylated form of HIF-1

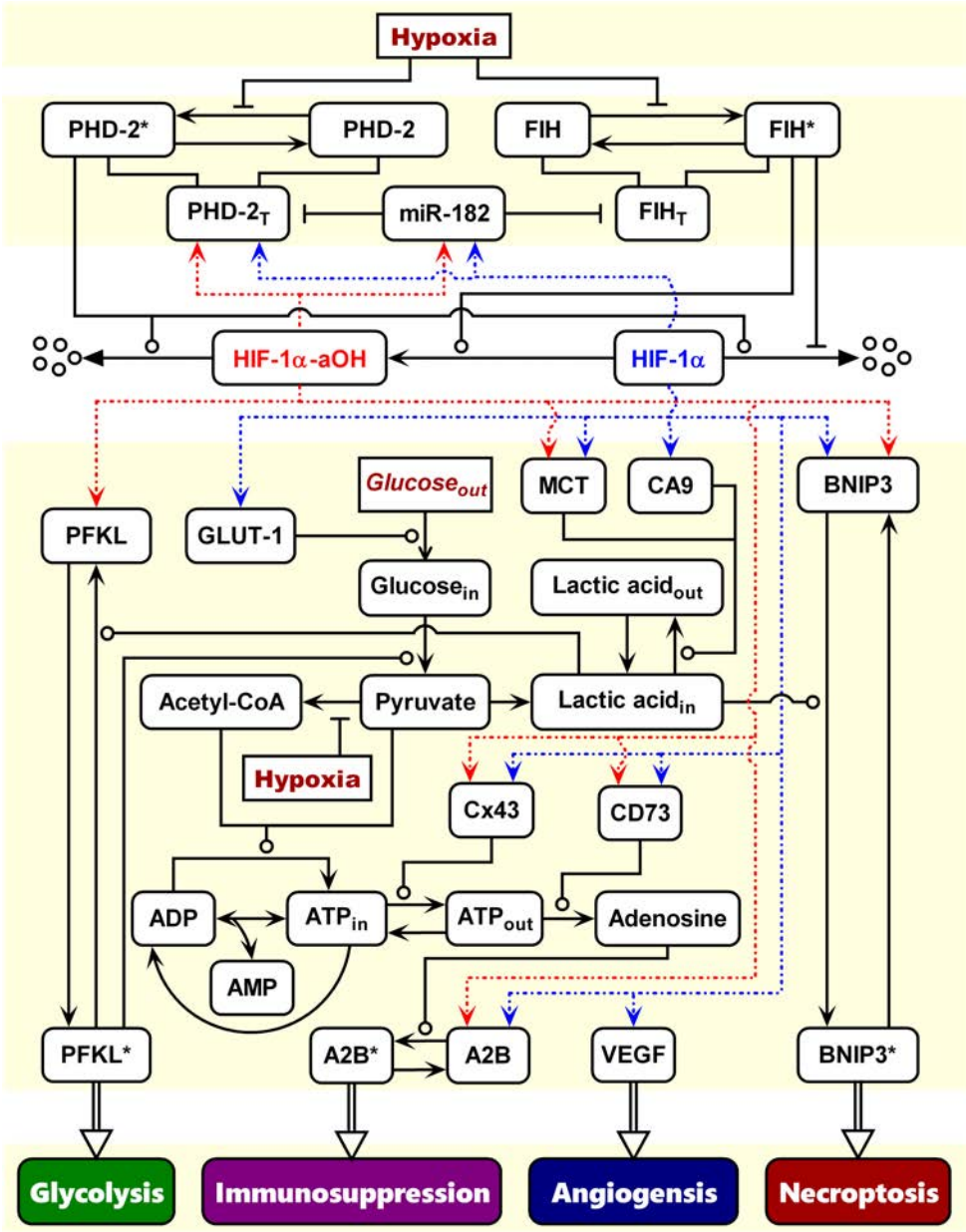

Fig. 1. Schematic of the integrated model. Upstream, the coupled HIF-1α-PHD-2 and HIF-1α-miR-182-PHD-2/FIH feedback loops regulate the stability and activity of HIF-1α. Downstream, PFKL, A2B, VEGF, and BNIP3 are indicators of altered energy metabolism, immunosuppression, angiogenesis, and necroptosis, respectively. HIF-1α-mediated transactivation of target genes is denoted by dashed lines. State transitions are labeled by arrow-headed solid lines. The promotion and repression of state transitions or interactions between proteins are represented by round- and bar-headed lines, respectively. Other processes are marked by hollow arrows.

for ubiquitination [11–13]. FIH* promotes the transition from HIF-1α to HIF-1α-aOH while inhibiting their PHD-2*-independent degradation [37]. PHD-2 is induced by both HIF-1α and HIF-1α-aOH, characterized by Hill functions (see Eq. 4 in the Supplementary Materials). The oxygen-dependent activation of hydroxylases (PHD-2 and FIH) and FIH*-dependent inhibition of HIF-1α degradation obey the Michaelis-Menten kinetics (see Eqs. 1, 5, and 8 in the Supplementary Materials).

Repression of PHD-2 and FIH production by miR-182

Although the role of miR-182 in tumor development is controversial, its carcinogenic function by promoting HIF-1α activation has been widely reported [20,21,42]. Typically, miR-182 targets the 3′-untranslated region of PHD-2 and FIH to activate HIF-1 indirectly [21], while HIF-1α induces miR-182 production, creating 2 positive feedback loops involving HIF-1α, PHD-2, FIH, and miR-182. Regardless of their status, PHD-2 and FIH were assumed to be down-regulated by miR-182 (see Eqs. 4 and 7 in the Supplementary Materials). Since hypoxia-dependent miR-182 up-regulation was found at 1% O_2 within the range of oxygen levels for HIF-1α-aOH activation [21], we assumed that both HIF-1α-aOH and HIF-1α can promote miR-182 production (see Eq. 3 in the Supplementary Materials).

Regulation of cellular pH by HIF-1α

The pH level of internal and external environments of tumor cells is regulated by HIF-1α in diverse manners. HIF-1α can lower pH by accelerating glycolysis, which leads to considerable accumulation of intracellular lactic acid. The production of glycolytic enzymes like PFKL and glucose transporters like GLUT1 is mediated by HIF-1α [10,43]. HIF-1α also scavenges intracellular H^+ by inducing MCT and CA9 since the former promotes the export of lactic acid and the latter neutralizes intracellular H^+ via increasing the production of HCO_3^- [44,45].

We simplified the characterization of lactic acid production, focusing on the underlying regulatory mechanism. Cellular uptake of glucose is facilitated by GLUT1, and active PFKL boosts the production of lactic acid from glucose. Lactic $acid_{in}$ (abbreviation, LA_{in}) and Lactic $acid_{out}$ (abbreviation, LA_{out}) represent the intracellular and extracellular lactic acid, respectively. MCT and CA9 promote the accumulation of LA_{out}. Since GLUT1 and CA9 are the FIH-inhibited targets of HIF-1α [27], their production rates were assumed to be proportional to the Hill function of the HIF-1α level (see Eqs. 15 and 11 in the Supplementary Materials). Because MCT was found to be induced at 1% O_2 [46], it was assumed to be induced by both HIF-1α-aOH and HIF-1α (see Eq. 12 in the Supplementary Materials).

Determination of different cellular outcomes

HIF-1α can induce glycolysis, immunosuppression, tumor angiogenesis, and necroptosis in response to hypoxia. As the critical rate-limiting enzyme involved in the only irreversible step in glycolysis, PFKL controls the conversion from fructose-6-P phosphorylation to fructose-1,6-bisphosphate [47]. Its enzymatic activity is highly dependent on pH and can be reduced by lowering the pH through allosteric regulation [48]. A slightly alkaline intracellular environment is optimal for maximizing PFKL activity [49]. Here, we differentiated 2 forms of PFKL, PFKL (inactive) and $PFKL^*$ (active), and their conversion is regulated by LA_{in} (Eqs. 8 and 9 in the Supplementary Materials).

Hypoxia also facilitates tumor cells to acquire immunosuppressive traits by pumping intracellular ATP out of the cells [50–52]. In the extracellular space, ATP is converted into adenosine monophosphate (AMP) by ectonucleoside triphosphate diphosphohydrolase 1 (CD39) and further catalyzed by ecto-5′-nucleotidase (CD73) to generate adenosine [53]. Studies show that excess extracellular adenosine activates the A2B adenosine receptor, promoting immunosuppression [54]. Furthermore, hypoxia enhances the expression of connexin 43 (Cx43) in tumor cell-derived exosomes, promoting ATP release [55–58]. Notably, Cx43 [57], CD73 [59], and A2B [60] are all target genes of HIF-1. We hypothesize that glucose is converted into pyruvate and acetyl-CoA to promote ATP production, while hypoxia inhibits the conversion of pyruvate into acetyl-CoA (Eqs. 18 to 20 in the Supplementary Materials). It was assumed that the interconversions among ATP, AMP, and ADP (adenosine diphosphate) follow the mass action law, and the total of their concentration is a constant ($[AXP_t]$) (Eqs. 24 to 26 in the Supplementary Materials). In this context, ATP is transported to the extracellular space via Cx43, converted into adenosine by CD73, and ultimately activates the A2B receptor (Eqs. 27, 29, and 31 in the Supplementary Materials). Given that mild hypoxia could induce the expression of Cx43, CD73, and A2B [57,59,60], the expression of these genes was assumed to be regulated by both HIF-1α and HIF-1α-aOH (Eqs. 23, 28, and 30 in the Supplementary Materials). Additionally, we assumed that adenosine promotes the conversion of A2B from its inactive to active form (Eqs. 30 and 31 in the Supplementary Materials).

HIF-1α induces VEGF and angiopoietin-2 (Ang-2) to regulate angiogenesis by directing the migration of mature endothelial cells to the hypoxic zone [61]. At the tip of the sprouts, endothelial cells use long filopodia in the receptors to sense VEGF [62]. Ang-2 is responsible for blocking Tie-2 signaling and increasing endothelial permeability to allow VEGF-induced cell migration [63]. For simplicity, we only considered VEGF as an effector in HIF-1α-dependent angiogenesis. Since VEGF belongs to the FIH-inhibited targets of HIF-1α [27], its synthesis is induced by fully activated HIF-1α alone (Eqs. 10 and 12 in the Supplementary Materials).

The hypoxic tumor tissue far from blood vessels shows a necrotic morphology [3]. This is mediated by HIF-1α-induced BNIP3, a member of non-FIH-inhibited targets [15]. Although mild hypoxia is sufficient to induce BNIP3 overexpression, cells are necrotic only under severe hypoxia. This mechanism may be involved in intracellular acidosis, which not only improves the stability of BNIP3 but also enhances its binding to the mitochondrial membrane, thereby activating its pronecrotic activity [28]. It was assumed that both forms of HIF-1α were responsible for BNIP3 induction. We considered 2 forms of BNIP3, i.e., BNIP3 (inactive form) and $BNIP3^*$ (active form), and the conversion from BNIP3 to $BNIP3^*$ is promoted by LA_{in} (Eqs. 13 and 14 in the Supplementary Materials).

Diverse cellular outcomes mediated by HIF-1α

To explore the adaptability of tumor cells to graded hypoxia, we showed the dynamics of different signaling components in the cellular response to hypoxia ($L_{O2} \leq 3\%$). Under mild hypoxia (e.g., $L_{O2} = 1.5\%$), HIF-1α accumulated and exhibited bell-shaped dynamics [Fig. 2A(a)]. Its total concentration, $[HIF\text{-}1\alpha_T]$, rapidly rose to a peak and then slowly returned to a level marginally higher than its initial expression. By contrast, $[PHD\text{-}2^*]$ dropped dramatically and then rose gradually toward saturation at a lower level. The restoration of $[PHD\text{-}2^*]$ was caused by the transcriptional up-regulation of PHD-2 by HIF-1α. In this case, the levels of active $PFKL^*$ and inactive A2B and BNIP3 rose prominently, while active $A2B^*$ increased initially but returned to basal levels over time, and VEGF and active $BNIP3^*$ remained at basal levels [Fig. 2B(a)]. This corresponds to a change in cellular metabolism from aerobic to anaerobic glycolysis. Indeed, compensating for oxygen deficiency by accelerating ATP production is a canonical adaptive response and is frequently preyed upon by tumors [64].

When the oxygen level decreased from 1.5% to 1%, PHD-2 activity further diminished, leading to a further increase in HIF-1α levels while maintaining the bell-shaped curve [Fig. 2A(b)]. While the moderate elevation in HIF-1α did not notably change the low expression levels of VEGF and $BNIP3^*$, it elevated the levels of PFKL and $A2B^*$ markedly, indicating that cells could start to initiate immunosuppressive functions [Fig. 2B(c)].

Under moderate hypoxia (e.g., $L_{O2} = 0.5\%$), $[HIF\text{-}1\alpha_T]$ was elevated remarkably compared with the case of mild hypoxia, while $[PHD\text{-}2^*]$ was down-regulated despite a slight change in $[PHD\text{-}2_T]$ [Fig. 2A(c)]. Thus, $[PFKL^*]$ increased further and [VEGF] rose moderately [Fig. 2B(c)]. Consequently, angiogenesis was triggered to promote tumor survival. This result suggests that in response to the aggravated loss of oxygen, cells would resort to additional strategies to adapt to hypoxia.

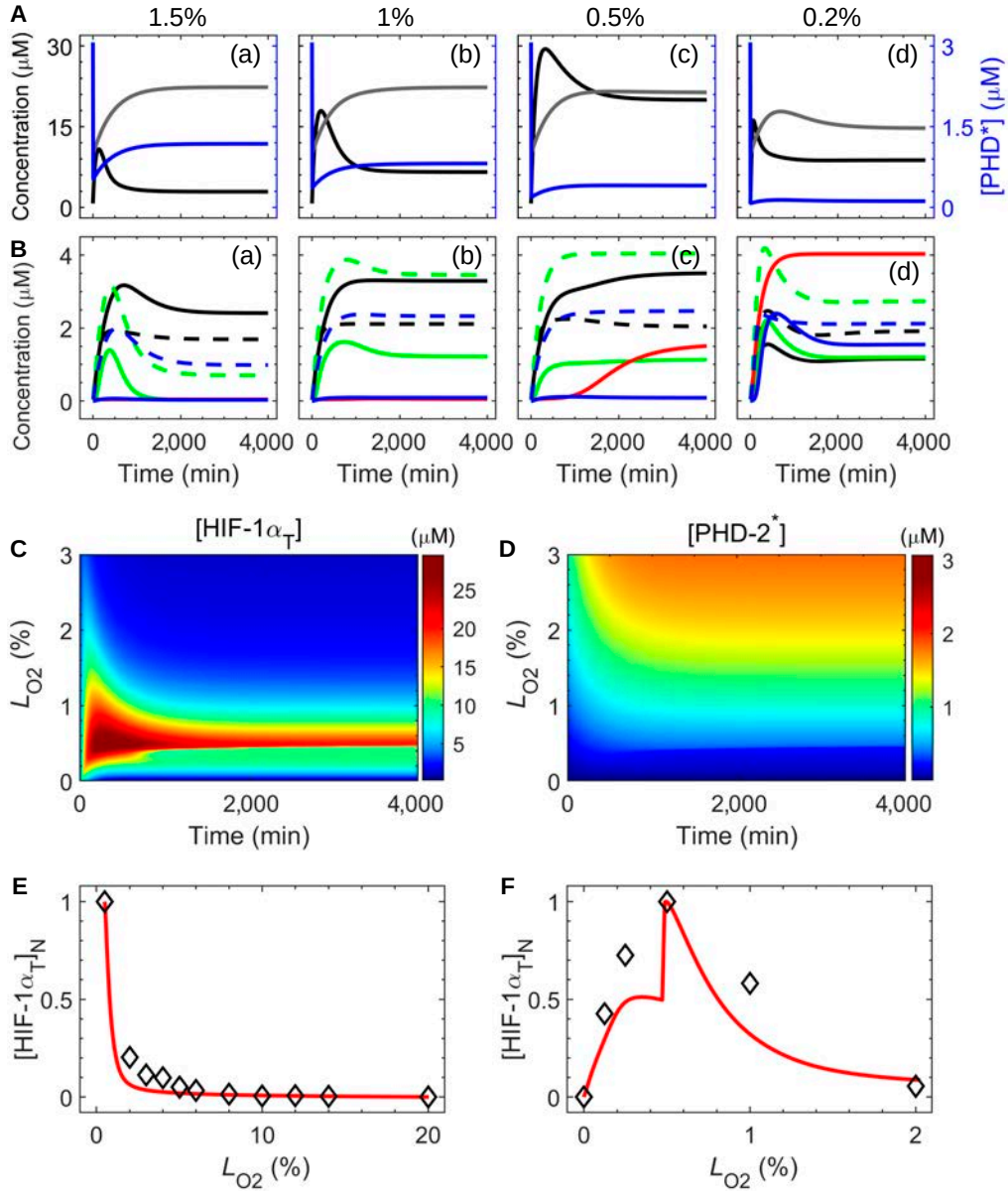

Fig. 2. Hypoxia-dependent cellular response mediated by HIF-1α. (A and B) Time courses of [HIF-1α_T] (black), [PHD-2*] (blue), and [PHD-2$_T$] (gray) (A), and of [PFKL] (black and dashed), [PFKL*] (black and solid), [A2B] (green and dashed), [A2B*] (green and solid), [VEGF] (red), [BNIP3] (blue and dashed), and [BNIP3*] (blue and solid) (B) for L_{O2} = 1.5 % (a), 1 % (b), 0.5 % (c), and 0.2 % (d). (C and D) Color-coded concentrations of HIF-1α_T (C) and PHD-2* (D) as a function of L_{O2} and time. (E and F) Steady-state value of [HIF-1α_T] normalized by its maximum versus L_{O2} [0.5 % to 20 % (E) and 0 % to 2 % O_2 (F)]. Red lines denote simulation results, while black squares refer to the experimental data from HeLa cells at 4 h [34]. [HIF-1α_T] indicates the total of [HIF-1α-aOH] and [HIF-1α]. The symbol [...]$_N$ stands for normalized concentration.

Under severe hypoxia (e.g., L_{O2} = 0.2 %), all 3 curves shifted downward compared with the case of L_{O2} = 0.5% [Fig. 2A(d)]. The down-regulation of HIF-1 may be associated with its destabilization due to the deactivation of FIH [37]. However, [A2B], [VEGF], and [BNIP3*] were still maintained at relatively high levels in contrast to low levels of [PFKL*] after the transients [Fig. 2B(d)]. Notably, BNIP3 was always strongly induced under hypoxia (Fig. 2B, blue) but was highly activated only during severe hypoxia, leading to cell necroptosis [Fig. 2B(d)] [45]. The coexistence of highly expressed VEGF and BNIP3* is consistent with the report that necroptosis provides a spatial structure for early angiogenesis [4].

Moreover, the color-coded time courses of [HIF-1α_T] and [PHD-2*] across L_{O2} were exploited to show the dependency of their dynamics on the extent of hypoxia (Fig. 2C and D). For L_{O2} > 1%, [HIF-1α_T] showed adaptive dynamics, while [PHD-2*] remained at high levels; for 0.5 % ≤ L_{O2} ≤ 1 %, [HIF-1α_T] reached rather high levels since PHD-2* dropped to low levels. In addition, we showed the dependency of the steady-state level of HIF-1α_T on L_{O2} (Fig. 2E and F). [HIF-1α_T] remained low for L_{O2} > 2 %, ensuring its inactivation under abundant oxygen; for 0.5 % ≤ L_{O2} ≤ 2 %, [HIF-1α_T] rose exponentially with decreasing L_{O2}, indicating its sensitivity to oxygen deficiency (Fig. 2E). When L_{O2} decreased from 2% to 0%, [HIF-1α_T] rose to its peak around 0.5 % O_2 followed by dropping to its basal levels due to its degradation in severe hypoxia (Fig. 2F) [37]. Our results are in good concordance with the experimental data [34].

Taken together, our model allows for the fine-tuning of HIF-1α dynamics, leading to an ordered selection of cellular outcomes depending on the severity of hypoxia. This selectivity may account for the morphological distribution of hypoxic tissues at different distances from blood vessels [3]. A broad area of tumor tissue is located close to the blood vessels, while the tumor tissue distant from the blood tissues undergoes necroptosis. Consistently, VEGF is mainly expressed around necrotic areas [65].

The hydroxylation status of HIF-1α determines its selection for different targets

HIF-1α-aOH and HIF-1α are partially and fully activated forms of HIF-1α, respectively, with different transcriptional activity. Their expression levels differed remarkably and predominated in different regimes of L_{O2}. [HIF-1α-aOH] was higher under mild and moderate hypoxia but declined to low levels under severe hypoxia (Fig. 3A). [HIF-1α-aOH] exhibited an adaptive response in each case, resulting from the negative feedback between HIF-1α-aOH and PHD-2. By contrast, [HIF-1α] was kept at low levels under mild and moderate hypoxia; it rose to intermediate levels under severe hypoxia (Fig. 3B).

To systematically show the dependence of HIF-1α expression on oxygen deficiency, we plotted the bifurcation diagrams of normalized [HIF-1α-aOH] and [HIF-1α] versus L_{O2} (Fig. 3C). There existed 2 saddle-node (SN) bifurcation points, implying that the dynamics of HIF-1α were governed by a bistable switch when L_{O2} was varied. With decreasing L_{O2}, [HIF-1α-aOH] rose along the upper branch; at SN_1, it jumped down to the lower branch. By contrast, [HIF-1α] climbed first along the lower branch until SN_1 and then switched to the upper branch. Of note, [HIF-1α] dropped to very low levels from the peak of the upper branch under anoxia due to the destabilization of HIF-1α. Thus, L_{O2} at SN_1 was a threshold for differentiating the predominance of HIF-1α-aOH over HIF-1α. These results further confirm that HIF-1α was activated progressively: HIF-1α-aOH was gradually activated under mild and moderate hypoxia, while HIF-1α was induced in severe hypoxia.

We further displayed the color-coded time courses of key molecules across L_{O2} in Fig. 3D to I. For $0.5\% \leq L_{O2} \leq 2\%$, HIF-1α-aOH was of sufficient expression, accompanied by a significant increase in both of [PFKL*] and [A2B*]. The response range of [PFKL*] was broader than that of [A2B*], suggesting that the cell first adjusts its energy metabolism and then initiates immunosuppression functions. [HIF-1α], [VEGF], and [BNIP3*] all remained at relatively high values for $0.2\% \leq L_{O2} < 0.5\%$, corresponding to the induction of angiogenesis and necroptosis. [HIF-1α] was kept at rather low levels for $L_{O2} < 0.2\%$, and apoptosis may be induced by the tumor suppressor p53, as reported in Ref. [66]. Thus, anaerobic glycolysis is first adopted by tumor cells to survive mild hypoxia, then angiogenesis is initiated to

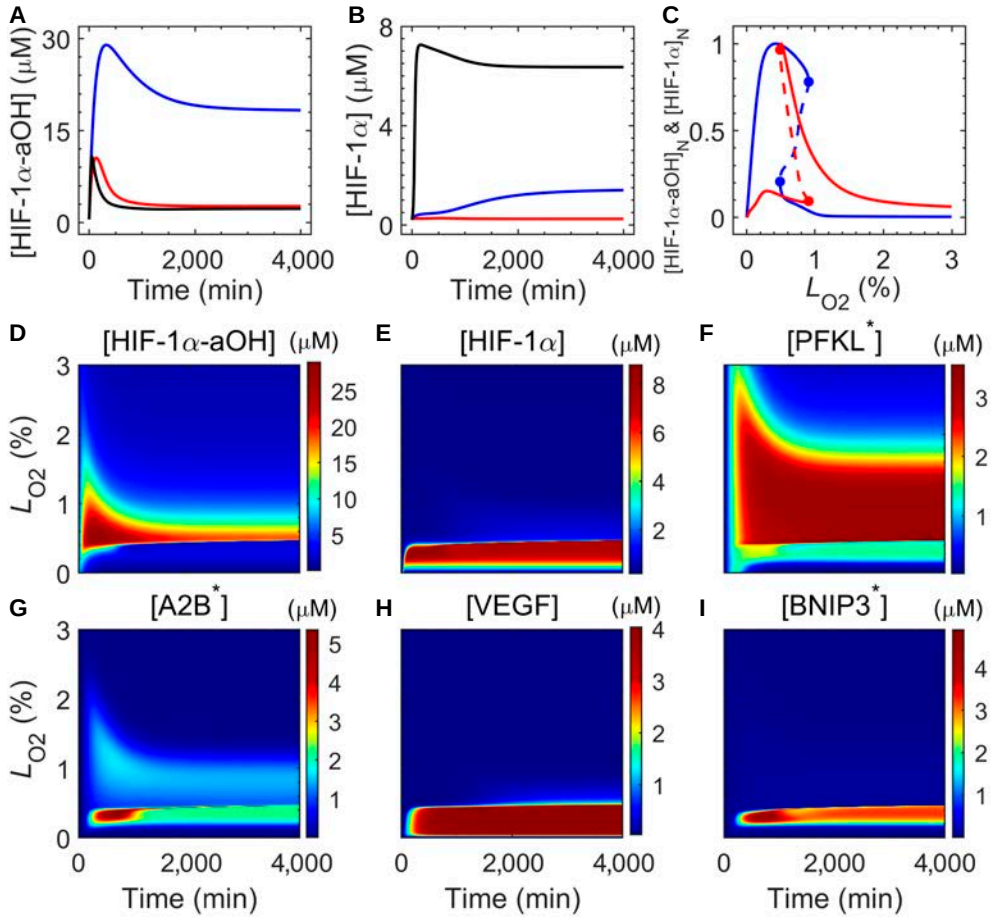

Fig. 3. The hydroxylation status of HIF-1α determines the selection of cellular outcome. (A and B) Temporal trajectories of [HIF-1α-aOH] (A) and [HIF-1α] (B) for $L_{02} = 1.5\%$ (red), 0.5% (blue), and 0.2% (black). (C) Bifurcation diagrams of normalized [HIF-1α] (blue) and [HIF-1α-aOH] (red) versus L_{02}. The stable and unstable steady states are denoted by solid and dashed lines, respectively. The subscript "N" indicates normalization. (D to I) Color-coded [HIF-1 α-aOH] (D), [HIF-1α] (E), [PFKL*] (F), [A2B*] (G), [VEGF] (H), and [BNIP3*] (I) as a function of L_{02} and time.

withstand moderate hypoxia, and necroptosis accompanied by angiogenesis is induced under severe hypoxia.

PHD-2 and FIH differentially regulate the hydroxylation status of HIF-1α

PHD-2 and FIH determine the hydroxylation status and activity of HIF-1α; it was worthwhile to clarify the underlying mechanism. Analysis of the network model revealed that the activity and concentration of these 2 hydroxylases were regulated by oxygen levels and their interaction network with miR-182 (Fig. 4A). In the bifurcation diagrams for [FIH*] and [PHD-2*] (Fig. 4B), there existed 2 SN bifurcation points. With decreasing L_{O2}, [PHD-2*] declined almost linearly (on the logarithm scale) along the upper branch, while [FIH*] remained unchanged until 1.5% O_2 and then dropped quickly; they both varied gradually along the lower branches. Thus, PHD-2 was more sensitive to mild hypoxia than FIH. Indeed, [PHD-2*] reached half its maximum at 2.17% O_2, around which initial accumulation of HIF-1α was observed experimentally [34], whereas [FIH*] halved at 0.68% O_2, which was close to L_{O2} at SN_1. Thus, the sequential inactivation of PHD-2 and FIH leads to the progressive activation of HIF-1α, and the transition involves the switch-like mechanism.

The oxygen concentration at SN_1 (SN_2) is denoted by L_{SN1} (L_{SN2}). L_{SN1} corresponds to the threshold of L_{O2} for full activation of HIF-1α, which is influenced by the rate constants for PHD-2

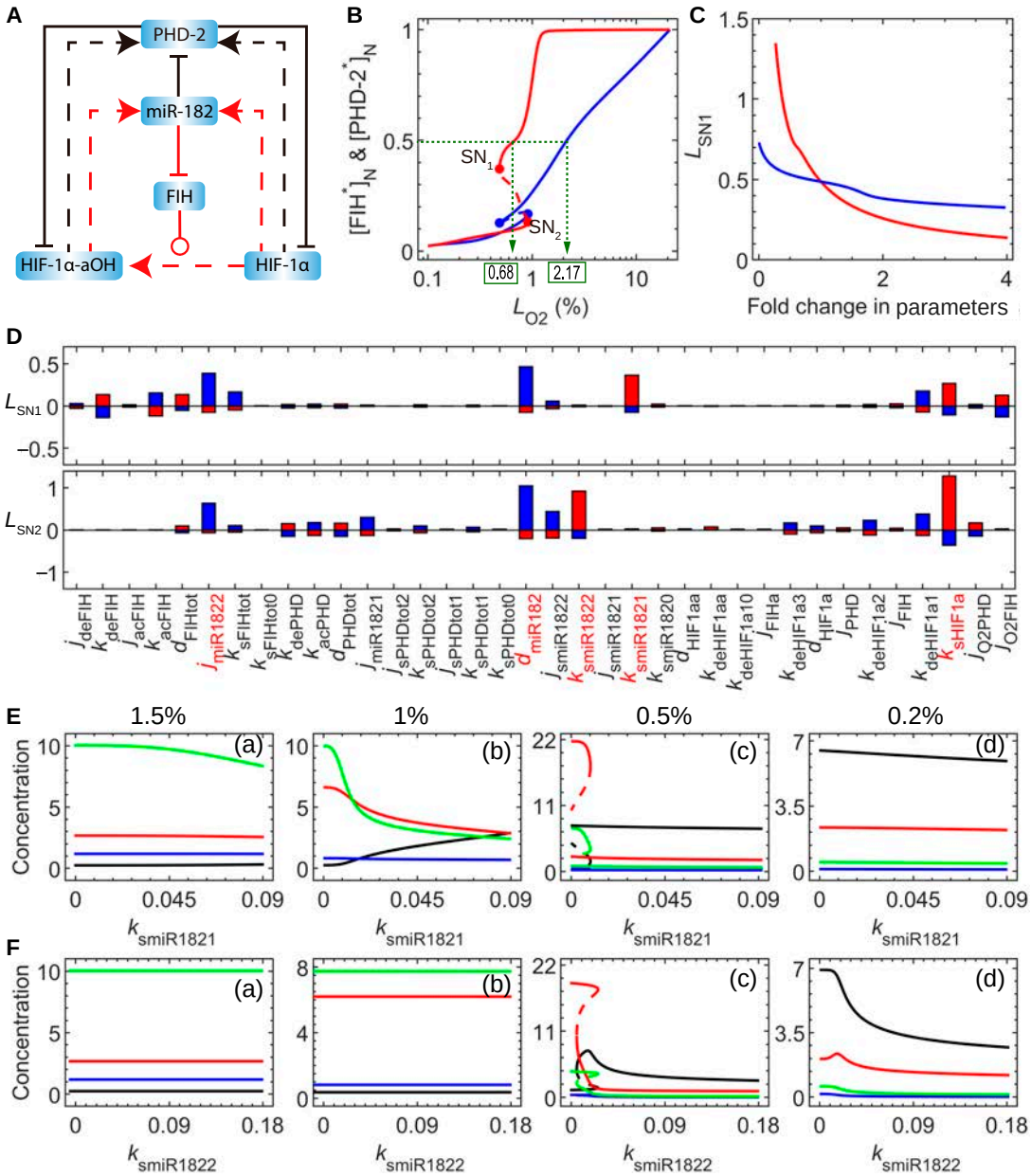

Fig. 4. Sequential induction of HIF-1α-aOH and HIF-1α by PHD-2 and FIH. (A) Simplified schematic of the interconnected HIF-1α/FIH/PHD-2/miR-182 loops. (B) Bifurcation diagrams for [FIH*] (red) and [PHD-2*] (blue) versus L_{O2}. [FIH*] and [PHD-2*] decay to half their initial concentrations at 0.68% and 2.17% O_2, respectively. (C) L_{SN1} as a function of fold change in k_{acPHD} (blue) or k_{acFIH} (red). (D) Percentage changes of L_{SN1} and L_{SN2} as each of the 36 parameters characterizing the coupled HIF-1α/FIH/PHD-2/miR-182 loops increases or decreases by 15% relative to the default value. (E and F) Bifurcation diagram of HIF-1α-aOH (red), HIF-1α (black), PHD-2* (blue), and FIH* (green) versus $k_{smiR1821}$ (E) and $k_{smiR1822}$ (F) for L_{O2} = 1.5% (a), 1% (b), 0.5% (c), and 0.2% (d).

and FIH activation, k_{acPHD} and k_{acFIH} (Fig. 4C). L_{SN1} rose slowly with increasing k_{acPHD}, whereas it changed sharply with k_{acFIH}. Thus, FIH (rather than PHD-2) could effectively modulate the transition from HIF-1α-aOH to HIF-1α. It was worth extending the above analysis to examine the sensitivity of L_{SN1} and L_{SN2} for FIH to changes in 36 parameter values (Fig. 4D). They were more sensitive to the following parameters: the rate constant of HIF-1 expression (k_{sHIF1a}), rate constants involved in miR-182 regulation ($k_{smiR1821}$, $k_{smiR1822}$ and $d_{smiR182}$), and the Michaelis constant of miR-182 for FIH inhibition ($j_{miR1822}$); these parameters were all associated with the interconnected loops between HIF-1α, HIF-1α-aOH, miR182, and FIH (red lines in Fig. 4A). Of note, HIF-1α-aOH and HIF-1α induced miR-182 to repress FIH expression, creating interlinked negative and positive feedback loops; they promoted the expression of PHD-2, facilitating their own degradation and enclosing 2 negative feedback loops (Fig. 4A).

We further investigated the influence of 2 production rates of miR-182 (HIF-1α-aOH-dependent and HIF-1α-dependent production rates separately denoted by $k_{smiR1821}$ and $k_{smiR1822}$) on [HIF-1α-aOH] and [HIF-1α] with worsening hypoxia. An elevation in either $k_{smiR1821}$ or $k_{smiR1822}$ led to a marked reduction in [FIH*] and promoted the conversion of HIF-1α-aOH to HIF-1α [Fig. 4E(b and c) and F(c)]. Under severe hypoxia, an increase in $k_{smiR1822}$ diminishes both [HIF-1α-aOH] and [HIF-1α] [Fig. 4F(d)]. This effect was due to a notable decrease in [FIH*] triggered by elevated [miR-182], which not only reduced the conversion rate of [HIF-1α] to [HIF-1α-aOH] but also compromised the stability of HIF-1α [Fig. 4F(d)]. Of note, the effects of the 2 production rates of miR-182 are negligible under different hypoxic conditions. Taken together, when other parameters take standard values, miR-182 mainly regulates HIF-1α via FIH instead of PHD-2.

miR-182 acts as a sliding regulator to release FIH-inhibited HIF-1 target genes under moderate hypoxia

The expression of miR-182 heavily relied on HIF-1α dynamics under different hypoxic conditions (Fig. 5A). [miR-182] exhibited adaptive dynamics due to the adaptation of HIF-1α to mild hypoxia. Under moderate hypoxia (e.g., 1 % O_2), [miR-182] rose toward saturation, consistent with experimental data [21]. [miR-182] reached rather high levels under severe hypoxia (e.g., 0.2 % O_2) due to the full activation of HIF-1α. In contrast, it dropped to rather low levels in anoxia due to down-regulation of HIF-1α (see Fig. 3).

In the bifurcation diagram for [miR-182], 2 SN bifurcation points appeared at the same L_{O2} as for [HIF-1α] [Fig. 5B(a)]. Correspondingly, PFKL, A2B, and BNIP3 were activated sequentially due to the progressive activation of HIF-1α, while the expression of VEGE was initiated in an exclusive region of $0.5\,\% \le L_{O2} \le 1\,\%$ [Fig. 5B(d)]. The bifurcation diagrams were shaped by 2 transcription rates, $k_{smiR1821}$ (by HIF-1α-aOH) and $k_{smiR1822}$ (by HIF-1α), which separately modulated the left and right arms in the HIF-1α/HIF-1α-aOH-miR182-FIH feedback loops (Fig. 4D). When $k_{smiR1822}$ was set to 0, i.e., blocking the

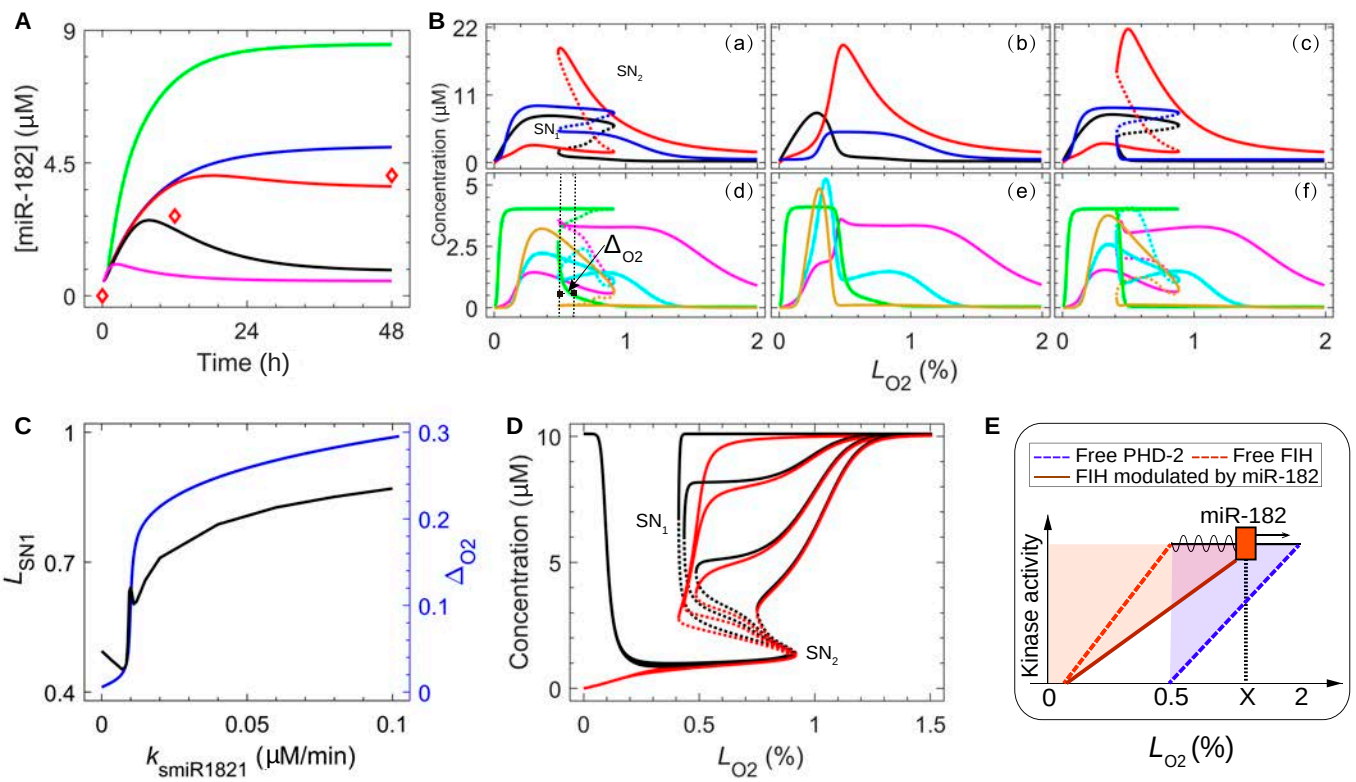

Fig. 5. Fine-tuning of HIF-1α activity by miR-182. (A) Time courses of [miR-182] under 1.5 % (black), 1 % (red), 0.5 % (blue), 0.2 % (green), and 0 % (magenta) O_2. Red squares represent the experimental data from DFO-treated PC-3 cells [21]. (B) Steady-state levels of [HIF-1α-aOH] (red, top), [HIF-1α] (black, top), and [miR-182] (blue, top), and [PFKL*] (magenta, bottom), [A2B*] (cyan, bottom), [VEGF] (green, bottom), and [BNIP*] (yellow, bottom) under default setting [(a) and (d)], $k_{smiR1822} = 0$ [(b) and (e)], and $k_{smiR1821} = 0$ [(c) and (f)]. (C) L_{SN1} (red) and Δ_{O2} (black) for [VEGF] as a function of $k_{smiR1821}$. (D) Steady-state levels of [FIH*] (red) and [FIH$_{tot}$] (black) for $k_{smiR1821} = 0$, 0.006, 0.009, and 0.012 (from left to right). (E) Schematic diagram depicting the role of miR-182 as a sliding regulator.

HIF-1α-miR182-FIH positive feedback loop, the bistability was replaced by monostability, and [miR-182] took low levels for $L_{O2} < 0.3\%$ [Fig. 5B(b)]. As a result, [BNIP3*] exhibited monostability and was unable to remain high over a wide range of oxygen levels [Fig. 5B(e)], inconsistent with the scenario for terminating unrescuable cells (e.g., apoptosis) [67]. That is, sufficient induction of miR-182 by fully activated HIF-1α is critical for the bistability in miR-182 expression as well as necroptosis under severe hypoxia. By contrast, the steady-state level of A2B* increased sharply till approximately 0.3 % O_2 [Fig. 5B(e)], indicating that under severe hypoxia, miR-182 loss may enhance HIF-1α expression by stabilizing FIH, which, in turn, drives a shift in cell fate from programmed necrosis to immunosuppression. This prediction could be experimentally validated by knocking out miR-182.

When $k_{smiR1821}$ was set to 0, i.e., the left arm of the HIF-1α-aOH-miR182-FIH negative feedback loop was disrupted, the bistability remained intact in the bifurcation diagram, but the lower branch of [miR-182] fell markedly [Fig. 5B(c)], while VEGF was induced synergetically with BNIP3* for $L_{O2} < 0.5\%$ [Fig. 5B(f)] and was down-regulated remarkably for $0.5\% \leq L_{O2} \leq 1\%$ compared with the normal case [Fig. 5B(d)]. That is, there was no exclusive L_{O2} range for HIF-1 to induce VEGF alone, which may decrease the possibility of tumor angiogenesis. The distance between L_{SN1} and L_{O2} at which [VEGF] reached one-fifth of its maximum was defined as Δ_{O2}, characterizing the difference in L_{O2} between VEGF production and BNIP3 activation. Δ_{O2} rose with increasing $k_{smiR1821}$ beyond 0.02, indicating that this exclusive induction of VEGF is greatly facilitated by the HIF-1α-aOH-mediated expression of miR-182 (Fig. 5C).

Notably, the divergence in VEGF expression and BNIP3 activation across L_{O2} ranges was related to the regulation of FIH by miR-182. Similar to [miR-182], both [FIH*] and [FIH_T] showed bistability under moderate hypoxia (Fig. 5D). For $k_{smiR1821} = 0$, both [FIH_T] and [FIH*] remained high along their upper branches and started to differ at 0.7 % O_2; with increasing $k_{smiR1821}$, the bifurcation point SN_1 shifted rightward and the bistability range shortened, while the upper branches were closer to each other and shifted downward (Fig. 5D). As L_{O2} decreased, FIH underwent 2 layers of regulation: a miR-182-mediated decrease in concentration ($0.7\% < L_{O2} < 1.2\%$) followed by a hypoxia-mediated decrease in activity ($< 0.7\%$). Thus, progressive deactivation of FIH* under worsening hypoxia leads to the gradual accumulation of fully activated HIF-1α, which sequentially induces VEGF and activates BNIP3.

Taken together, miR-182 can be considered a sliding regulator of the hypoxia switch. As shown in the cartoon (Fig. 5E), active FIH and PHD-2 were remarkably down-regulated around 0.5 % and 2 % O_2 (Fig. 4A), respectively, while miR-182 had a regulatory role over $0.5\% \leq L_{O2} \leq 1.2\%$ (Fig. 5D), promoting the functioning of fully activated HIF-1α, such as driving angiogenesis by destroying FIH.

Hypoxia degree-dependent acidic microenvironment formation and acidosis-activated necroptosis

Tumor cells can create a survival-friendly acidic microenvironment under hypoxia, depending on the amount and distribution of lactic acid [45]. Excessive intracellular lactic acid can be lethal to hypoxic cells and lead them to necroptosis. [LA_{in}] and [LA_{out}] denote the concentrations of lactic acid inside and outside the cell, respectively. We hypothesized that sufficient LA_{in} could cause acidosis and thus necrotize cells, while sufficient LA_{out} implied the establishment of an acidic microenvironment.

We first examined how the concentration and distribution of lactic acid were correlated with the severity of hypoxia. Under mild hypoxia, [LA_{in}] was greater than [LA_{out}] [Fig. 6A(a)] due to initially accelerated glycolysis characterized by a remarkable increase in [PFKL*] [Fig. 6B(a)]; the increase in [MCT] promoted the export of lactic acid. Under moderate hypoxia, [LA_{out}] predominated in the later phase of the response [Fig. 6A(b)]. This was associated with increases in [PFKL*], [CA9], and [MCT]; the former induced the production of lactic acid, while the latter two promoted its extracellular localization to form an acidic microenvironment [Fig. 6B(b)].

Under severe hypoxia, both [LA_{in}] and [LA_{out}] increased several-fold [Fig. 6A(c)], accompanied by increases in [GLUT1], [Glucose], [CA9], and [MCT] [Fig. 6B(c)]. The GLUT1-mediated increase in glucose uptake further activated the glycolytic pathway, responsible for massive accumulation of lactic acid; meanwhile, enhanced CA9 and MCT production facilitated LA_{out} accumulation. This could further increase the acid concentration in the microenvironment, and the tumor cell itself could become necrotic due to acidosis-activated BNIP3 caused by high [LA_{in}].

The moderate increases in [LA_{in}] and [LA_{out}] evoked an acidic microenvironment under moderate hypoxia (see region II in Fig. 6C); by contrast, their remarkable increases resulted in acidosis under severe hypoxia (see region I). We further dissected the contribution of each regulator (including PFKL, GLUT1, MCT, and CA9) by setting their respective synthesis rates to 0 (control case); $\Delta_{LA_{in}}$ and $\Delta_{LA_{out}}$ separately denoted the changes in [LA_{in}] and [LA_{out}] relative to the control case (Fig. 6D). PFKL deficiency led to decreases in [LA_{in}] and [LA_{out}] across hypoxia, whereas GLUT1 deficiency led to their reduction only under severe hypoxia. This difference suggests that cells activate distinct pathways to enhance glycolysis and avoid high intracellular acidity when faced with different degrees of hypoxia (Fig. 6D). MCT acts as a generic scavenger across hypoxia; when its production was blocked, the decrease in [LA_{in}] was always accompanied by an increase in [LA_{out}]. By contrast, CA9 is a specific scavenger, and its deletion elicited an increase in [LA_{in}] and a decrease in [LA_{out}] mainly under severe hypoxia.

Under severe hypoxia, the competition between GLUT1 and CA9 affected the intracellular pH and BNIP3 activation. Both [LA_{in}] and [LA_{out}] rose with increasing k_{sGLUT1} (production rate of GLUT1) [Fig. 6E(a) and (b)], while a profound LA_{in}-to-LA_{out} shift occurred at larger k_{sCA9} (production rate of CA9) values. BNIP3 activation was modulated by both GLUT1 and CA9. At small or moderate k_{sGLUT1}, BNIP3* accumulation was repressed due to the pumping of H^+ by CA9; BNIP3* was sufficiently activated at large k_{sGLUT1} when excessive lactic acid accumulated in cells, leading to cell necroptosis [Fig. 6E(c)].

These results suggest that cells utilize several pathways to enhance glycolysis, thereby ensuring sufficient energy production and preventing acidosis. The accumulation of acid in internal or external environments depends on the severity of hypoxia and the selective expression of target genes of HIF-1 (Fig. 6F). Mildly hypoxic cells use HIF-1α-aOH to induce mild expression of PFKL, leading to weak accumulation of intracellular acid; meanwhile, moderately induced MCT exports small amounts of H^+. Under moderate hypoxia, HIF-1α-aOH is markedly elevated, leading to enhanced PFKL expression and intracellular

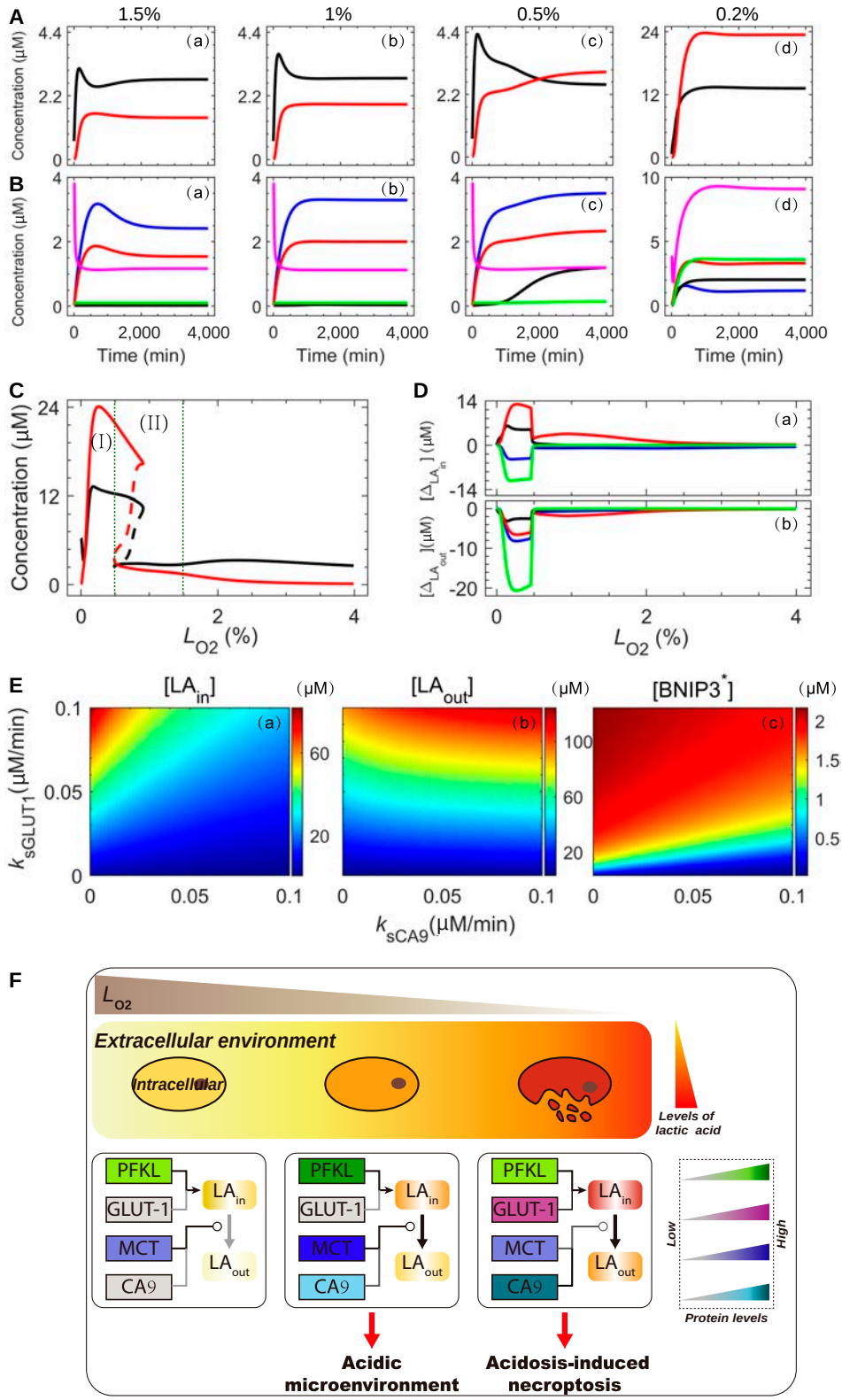

Fig. 6. The level of lactic acid determines the formation of an acidic microenvironment or acidosis-induced necroptosis. (A and B) Time courses of $[LA_{in}]$ (black) and $[LA_{out}]$ (red) in (A), and $[PFKL^*]$ (blue), [CA9] (black), [MCT] (red), [GLUT-1] (green), and [Glucose] (magenta) in (B) for $L_{O2} = 1.5\,\%$ (a), 1 % (b), 0.5 % (c), and 0.2 % (d). (C) Steady-state values of $[LA_{in}]$ (black) and $[LA_{out}]$ (red) versus L_{O2}. (D) Effects of separately deleting PFKL (blue), CA9 (black), MCT (red), and GLUT1 (green) on steady-state values of $[LA_{in}]$ (a) and $[LA_{out}]$ (b). (E) Steady-state levels of LA_{in} (a), LA_{out} (b), and $BNIP3^*$ (c) versus the parameter pair (k_{sGLUT1} and k_{sCA9}) for $L_{O2} = 0.2\,\%$. (F) Schematic of the cellular distribution of lactic acid under mild ($1\,\% < L_{O2} \leq 2\%$), moderate ($0.5\,\% < L_{O2} \leq 1\%$) and severe ($L_{O2} < 0.5\,\%$) hypoxia (from left to right) and the corresponding activated pathways.

acid accumulation; coexpression of MCT and CA9 results in a large amount of H^+ spillover, promoting the formation of acidic environment. Severely hypoxic cells further increase inward glucose transport by enhancing GLUT1 production, while elevated expression of CA9 and MCT further neutralizes intracellular H^+. If CA9 fails to counteract the massive GLUT1-induced intracellular accumulation of H^+, acidosis-dependent necroptosis will be triggered.

Discussion and Conclusion

The hierarchical hypoxic microenvironment in solid tumors leads to heterogeneous responses to hypoxia in tumor cells, such as inducing an immune-resistant quiescent state in some cells and promoting tumor metastasis through the formation of highly permeable tumor blood vessels [6,68]. However, how tumor cells autonomously regulate their signaling networks to adapt to varying degrees of hypoxia remains an unresolved issue. Given that HIF-1 is a key regulator of the hypoxic response and produces typical morphological differences in tumor tissues, our study developed a network model to reveal how tumor cells utilize the HIF-1 signaling pathway to adapt to graded hypoxia. HIF-1 is progressively activated due to the modulation of its activity by oxygen level-dependent hydroxylases PHD-2/FIH and their regulators (e.g., miR-182); consequently, representative adaptive processes, including altered energy metabolism, immunosuppression, angiogenesis, and necroptosis, occur sequentially with worsening hypoxia when cells are distant from the blood vessels (Fig. 7). From a network perspective, the progressive induction of different responses depends on the selective activation of downstream signaling pathways, guided by the interconnected feedback loops involving HIF-1α, PHD-2, FIH, and miR-182, establishing an autonomous hypoxia-adaptive mechanism. This mechanism also orchestrates multiple aspects of anaerobic glycolysis including glucose absorption and the production and export of acid to ensure substantial ATP generation for cellular survival, while sustaining an acidic tumor microenvironment.

miRNAs can play a prominent role in the modulation of HIF-1-dependent cellular adaptation to hypoxia. miR-182 exemplifies a category of miRNAs that are induced by HIF-1 and subsequently modulate HIF-1 through the hydroxylases PHD-2 and FIH, thereby enclosing multiple feedback loops. As indicated in this work, miR-182 potentially acts as a modulator, facilitating VEGF induction (tumor angiogenesis) across defined hypoxic conditions [21]. miR-182 plays a role in a variety of processes, including proliferation, apoptosis, differentiation, glucose metabolism, invasion, and metastasis [20,69–71]. Moreover, a variety of factors including MINT3 [72], PKD-1 [17], miR-351 [73], and miR-210 [74] are also involved in HIF-1 regulation by targeting PHD-2 and FIH. It is intriguing to investigate how miR-182 synergizes with other enzymatic regulators to modulate HIF-1 signaling.

Considering the feedback loops involving HIF-1α, miR-182, PHD-2, and FIH, we underscore the crucial role of miR-182 in regulating VEGF in response to hypoxia. Indeed, other HIF-1α-induced miRNAs also play important roles in the hypoxic response [75]. For instance, HIF-1α induces miR-155 to relieve its activity during prolonged hypoxia [19], while miR-122 enhances hepatic ischemia tolerance by promoting hepatic protection through a feedback mechanism that enhances PHD-1 inhibition [76]. Moreover, HIF-2α plays a remarkable role in

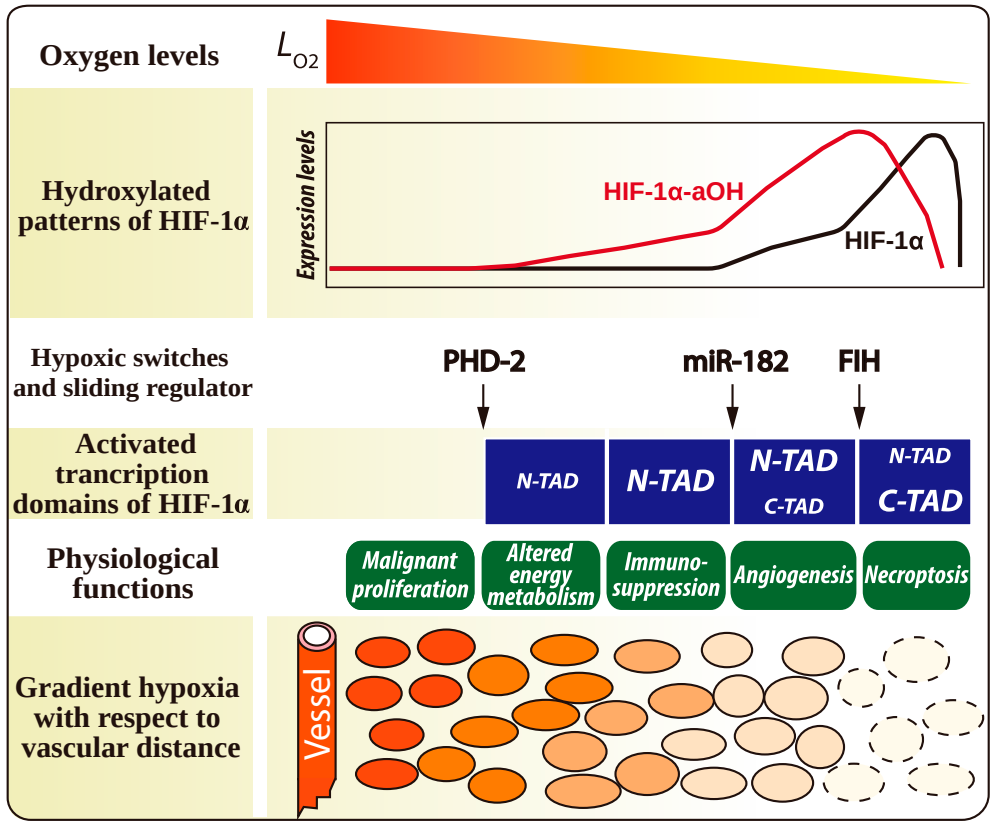

Fig. 7. Schematic of the HIF-1α-mediated cellular response to graded hypoxia. The intensity of the filled colors in the bottom row is associated with the oxygen levels.

hypoxic response by transactivating some miRNAs. For example, HIF-2α induces the expression of miR-29a in $CD4^+$ cells, which is crucial for alleviating TH1-mediated inflammatory responses [77]. In the future, including more miRNAs in the network model of the hypoxic response may provide valuable insights for the precise treatment of various diseases.

Sufficient activation of BNIP3 is responsible for hypoxic necroptosis, in which BNIP3 dimerizes and inserts into the mitochondrial membrane to regulate its permeability [78,79]. Although BNIP3 is expressed at various hypoxia levels, it induces cell necroptosis only under severe hypoxia, establishing a scenario in which the expression and activation of BNIP3 are separately regulated [27,45]. This could result from the difficulty in inducing acidosis under mild hypoxia when lactic acid production is negligible. In the absence of acidosis, BNIP3 is unstable and exhibits low affinity to mitochondria [28]. Alternatively, only when BNIP3 accumulates sufficiently can it counteract the formation of heterodimers with Bcl-2, Bcl-xL, or Bax; indeed, the expression of BNIP3 in severe hypoxia is nearly twice that observed in mild hypoxia [27,28,80]. In addition, BNIP3 could also promote cell survival through autophagy, which emerges under moderate hypoxia [81].

The role of necroptosis in tumor progression is worth discussing. As an essential hallmark of aggressive tumors, necroptosis promotes cell survival by amplifying HIF-1α signaling as well as activating the NF-κB and PI3K/mTOR pathways [82]. Consistently, necrotic extracts from dying cells promote migration and invasion of glioblastoma cancer stem cells with reduced oxygen tension [83]. Necrotic lysates enhance endothelial cell proliferation and angiogenesis, promoting cell invasion and migration [84]. Thus, necroptosis may be a strategy for tumor progression, and the necroptosis of individual cells facilitates more robust survival of the tumor cell community. Considering the role of necrotic lysates in promoting tumor vascularization, a cross-link between VEGF and necrotic downstream pathways could be identified [82]. It would be interesting to take into account the inflammatory regulatory pathways to clarify the mechanisms underlying the coordination of necroptosis, inflammation, and hypoxia in tumor progression [83,85–87]. Following VEGF-mediated neovascularization, HIF-1 signaling is attenuated with elevated oxygen pressure, creating a long-range feedback loop between HIF-1, VEGF, and hypoxia detection. Integrating this loop into our model is challenging but intriguing since a considerable portion of tumor cells are subjected to at least 2 cycles of hypoxia [88].

Our results suggest that cell necroptosis could be avoided by disrupting the expression and activation of BNIP3 or HIF-1 under severe hypoxia. FIH inhibitors could be exploited to destabilize HIF-1α since FIH contributes to the stabilization of HIF-1α under hypoxia [37]. Alternatively, p53 may be a candidate for inhibiting necroptosis for the following reasons: (a) p53 directly inhibits BNIP3 expression [89]; (b) p53 reduces HIF-1 activity by competing for p300 and induces Mdm2 production to degrade HIF-1 [90,91]; and (c) multiple targets of p53 are associated with the inhibition of glycolysis, which disrupts acidosis and BNIP3 activation [92]. Probing the interplay between p53 and HIF-1 revealed a mechanism for activating p53 under severe hypoxia [93]. Replacing BNIP3-mediated necroptosis with p53-mediated apoptosis may be a viable approach for tumor suppression.

Our findings could be validated by designing experiments specifically. Based on the experiment conducted by Dayan et al. [27], devising experiments that encompass HIF-1 target genes within our model across varying oxygen concentrations could provide validation for our findings regarding the relationship between target gene expression and the degree of hypoxia. To further investigate the role of miR-182 in regulating VEGF expression under hypoxia, it is advisable to knock out miR-182 and assess VEGF expression under different oxygen levels. In addition, the effects of oxygen levels on the expression and activation of BNIP3 could be tested indirectly by assessing the key downstream components involved in the BNIP3-mediated necroptosis pathway, such as RIPK1, RIPK3, and MLKL [78,79]. Inhibiting these factors to promote cell survival could clarify whether BNIP3 activity is markedly enhanced under severe hypoxia.

Our work could provide insight into the mechanism underlying tumor cell adaptation to hypoxia, but some limitations still exist. First, a critical assessment of the model's simplifications against real biological processes is essential. For example, we did not include the neuronal guidance protein Netrin-1, which is a noteworthy target of HIF-1 [53]. Incorporating Netrin-1 into the model could enhance the comprehension of the regulatory details of immunosuppression and energy metabolism. Second, we omitted another HIF, HIF-2α, which performs different functions compared to HIF-1α. It has been reported that HIF-1α and HIF-2α have distinct transcriptional targets: the former primarily induces genes involved in glycolysis in response to acute hypoxia, whereas the latter regulates genes related to erythropoietin under chronic hypoxia [94]. Moreover, they also cooperatively induce genes such as VEGF and GLUT-1 [94]. Incorporating HIF-2α into the model would contribute to understanding how cells utilize HIF pathways to adapt to hypoxia. Third, the crosstalk between HIF-1 and NF-κB is not included in our model [95]. Their interaction is frequently observed in the hypoxic response. For example, NF-κB can act as a transactivator of HIF-1α [96]. They also cooperate to induce genes such as interleukin-6, cyclooxygenase-2, and matrix metalloproteinase-9 [95]. Including NF-κB in the model could help elucidate how hypoxia triggers chronic inflammation through the HIF-1α-NF-κB interaction. In addition, biological noise is not considered in the present model [97]. Kang et al. [98] proposed a theoretical framework for the stochastic dynamics of the HIF-1 network based on landscape topography. Incorporating their scheme into our research could provide valuable insights into the significance of stochasticity in cellular adaptation to hypoxia.

Our results may provide clues for treating hypoxia-associated diseases. Therapeutic strategies targeting HIF can be classified as HIF stabilizers and inhibitors tailored in different diseases [99]. HIF stabilizers up-regulate the α subunit of HIFs by inhibiting PHDs, primarily used to treat anemia caused by hypoxia [100,101]. In contrast, HIF inhibitors block the dimerization of HIF subunits, mainly used in cancer therapy to inhibit tumor growth in clear cell renal carcinoma [102]. However, in patients with both ischemic cardiovascular disease and cancer, HIF inhibitors may interfere with blood flow restoration, potentially exacerbating tissue damage [103]. Given the selective expression of genes targeted by HIF-1α, optimal treatment strategies could be developed by concurrently targeting multiple factors and accounting for interpatient variability. The proposed model elucidates how inhibition of HIF-1 regulatory factors, including hydroxylases and miR-182, selectively attenuates distinct hypoxic responses, such as angiogenesis and immunosuppression.

Methods

Based on the typical morphological features observed in tumor tissue at varying distances from blood vessels, glycolysis, immunosuppression, angiogenesis, and necroptosis were selected as 4 representative processes in response to hypoxia [3]. HIF-1 has been shown to transcriptionally regulate several enzymes involved in the induction of glycolysis [24]. For simplicity, PFKL was selected as a marker for the transition from oxidative metabolism to glycolysis [27]. Considering the role of BNIP3 in necroptosis and the role of VEGF in angiogenesis at the periphery of tumor necrotic regions, VEGF and BNIP3 were chosen as markers for angiogenesis and necroptosis, respectively [3,28]. In addition, miR-182 and the pH-regulating factors MCT and CA9 were also considered in the regulation of these processes [21,45].

Besides the input (hypoxia) and 4 outputs (glycolysis, immunosuppression, angiogenesis, and necroptosis), the model consists of 31 nodes and is mathematically characterized by 28 ordinary differential equations (ODEs). The concentration of each species (denoted as [...]) is described by the state variables in the ODEs, with their detailed definitions provided in Supplementary Method S1. In the model, the enzyme-catalyzed reactions are characterized by Michaelis-Menten kinetics while HIF-1α-dependent transcription of the target genes is described by the Hill functions. In addition, protein degradation follows the law of mass action. The definition and initial values of each variable and parameter are listed in Tables S1 and S2, respectively. Of note, besides the parameters based on experimental results, other parameters in the model are estimated through trial and error to ensure that the simulation results are consistent with experimental observations (see Table S2 for details). Moreover, a sensitivity analysis was performed to ensure the model's robustness to perturbations in parameter values (as shown in Fig. 4D). Oscill8 was used to solve the ODEs and perform single- and 2-parameter bifurcation analysis. The value of oxygen level L_{O2} corresponds to the percentage of oxygen volume in the air. The initial value of each variable was set to its steady-state value at 21% O_2. Time is in units of minutes.

Acknowledgments

Funding: This work was supported by the National Natural Science Foundation of China (nos. 12090052, 11874209, 11574139, and 11934008). The authors also thank the support of the High Performance Computing Center of Nanjing University.
Author contributions: X.-P.Z., F.L., and W.W. conceived and designed the project. P.W. performed the study. P.W., X.-P.Z., F.L., and W.W. wrote the paper. All authors analyzed the data and read/edited the paper.
Competing interests: The authors declare that they have no competing interests.

Data Availability

All data needed to evaluate the conclusions are presented in the paper and the Supplementary Materials. Custom codes will be available upon request to X.-P.Z. (Email: zhangxp@nju.edu.cn).

Supplementary Materials

Supplemental Method S1
Tables S1 and S2

References

1. Gilkes DM, Semenza GL, Wirtz D. Hypoxia and the extracellular matrix: Drivers of tumour metastasis. *Nat Rev Cancer*. 2014;14(6):430–439.
2. Spencer JA, Ferraro F, Roussakis E, Klein A, Wu J, Runnels JM, Zaher W, Mortensen LJ, Alt C, Turcotte R, et al. Direct measurement of local oxygen concentration in the bone marrow of live animals. *Nature*. 2014;508(7495):269–273.
3. Beasley NJ, Wykoff CC, Watson PH, Leek R, Turley H, Gatter K, Pastorek J, Cox GJ, Ratcliffe P, Harris AL. Carbonic anhydrase IX, an endogenous hypoxia marker, expression in head and neck squamous cell carcinoma and its relationship to hypoxia, necrosis, and microvessel density. *Cancer Res*. 2001;61(13):5262–5267.
4. Zhao X, Sun B, Liu Y, Zhang D, Liu Z, Zhao X, Gu Q, Han C, Dong X, Che N, et al. Linearly patterned programmed cell necrosis induced by chronic hypoxia plays a role in melanoma angiogenesis. *J Cancer*. 2016;7(1):22–31.
5. Giatromanolaki A, Koukourakis MI, Sivridis E, O'Byrne K, Gatter KC, Harris AL. 'Invading edge vs. inner' (edvin) patterns of vascularization: An interplay between angiogenic and vascular survival factors defines the clinical behaviour of non-small cell lung cancer. *J Pathol*. 2000;192(2):140–149.
6. Edmondson R, Broglie JJ, Adcock AF, Yang L. Three-dimensional cell culture systems and their applications in drug discovery and cell-based biosensors. *Assay Drug Dev Technol*. 2014;12(4):207–218.
7. Rankin EB, Giaccia AJ. Hypoxic control of metastasis. *Science*. 2016;352(6282):175–180.
8. Wang GL, Jiang BH, Rue EA, Semenza GL. Hypoxia-inducible factor 1 is a basic-helix-loop-helix-PAS heterodimer regulated by cellular O2 tension. *Proc Natl Acad Sci*. 1995;92(12):5510–5514.
9. Semenza GL. HIF-1 and mechanisms of hypoxia sensing. *Curr Opin Cell Biol*. 2001;13(2):167–171.
10. Semenza GL. Targeting HIF-1 for cancer therapy. *Nat Rev Cancer*. 2003;3(10):721–732.
11. Schofield CJ, Ratcliffe PJ. Oxygen sensing by HIF hydroxylases. *Nat Rev Mol Cell Biol*. 2004;5(5):343–354.
12. Marxsen JH, Stengel P, Doege K, Heikkinen P, Jokilehto T, Wagner T, Jelkmann W, Jaakkola P, Metzen E. Hypoxia-inducible factor-1 (HIF-1) promotes its degradation by induction of HIF-α-prolyl-4-hydroxylases. *Biochem J*. 2004;381(Pt 3):761–767.
13. Jaakkola P, Mole DR, Tian YM, Wilson MI, Gielbert J, Gaskell SJ, von Kriegsheim A, Hebestreit HF, Mukherji M, Schofield CJ, et al. Targeting of HIF-α to the von Hippel-Lindau ubiquitylation complex by O_2-regulated prolyl hydroxylation. *Science*. 2001;292(5516):468–472.
14. Mahon PC, Hirota K, Semenza GL. FIH-1: A novel protein that interacts with HIF-1 alpha and VHL to mediate repression of HIF-1 transcriptional activity. *Genes Dev*. 2001;15(20):2675–2686.
15. Dayan F, Monticelli M, Pouysségur J, Pécou E. Gene regulation in response to graded hypoxia: The non-redundant roles of the oxygen sensors PHD and FIH in the HIF pathway. *J Theor Biol*. 2009;259(2):304–316.
16. Koivunen P, Hirsila M, Gunzler V, Kivirikko KI, Myllyharju J. Catalytic properties of the asparaginyl hydroxylase (FIH) in the oxygen sensing pathway are distinct from those of its prolyl 4-hydroxylases. *J Biol Chem*. 2004;279(11):9899–9904.

17. Fábián Z, Taylor CT, Nguyen LK. Understanding complexity in the HIF signaling pathway using systems biology and mathematical modeling. *J Mol Med*. 2016;94(4):377–390.
18. Serocki M, Bartoszewska S, Janaszak-Jasiecka A, Ochocka RJ, Collawn JF, Bartoszewski R. miRNAs regulate the HIF switch during hypoxia: A novel therapeutic target. *Angiogenesis*. 2018;21(2):183–202.
19. Bruning U, Cerone L, Neufeld Z, Fitzpatrick SF, Cheong A, Scholz CC, Simpson DA, Leonard MO, Tambuwala MM, Cummins EP, et al. MicroRNA-155 promotes resolution of hypoxia-inducible factor 1α activity during prolonged hypoxia. *Mol Cell Biol*. 2011;31(19):4087–4096.
20. Wang M, Wang W, Wang J, Zhang J. MiR-182 promotes glucose metabolism by upregulating hypoxia-inducible factor 1α in NSCLC cells. *Biochem Biophys Res Commun*. 2018;504:400–405.
21. Li Y, Zhang D, Wang X, Yao X, Ye C, Zhang S, Wang H, Chang C, Xia H, Wang YC, et al. Hypoxia-inducible miR-182 enhances HIF1α signaling via targeting PHD2 and FIH1 in prostate cancer. *Sci Rep*. 2015;5:12495.
22. Peng X, Gao H, Xu R, Wang H, Mei J, Liu C. The interplay between HIF-1α and noncoding RNAs in cancer. *J Exp Clin Cancer Res*. 2020;39(1):27.
23. Cerychova R, Pavlinkova G. HIF-1, metabolism, and diabetes in the embryonic and adult heart. *Front Endocrinol*. 2018;9:460.
24. Makanji Y, Tagler D, Pahnke J, Shea LD, Woodruff TK. Hypoxia-mediated carbohydrate metabolism and transport promote early-stage murine follicle growth and survival. *Am J Physiol Endocrinol Metab*. 2014;306(8):E893.
25. Denko NC. Hypoxia, HIF1 and glucose metabolism in the solid tumour. *Nat Rev Cancer*. 2008;8(9):705–713.
26. Kim JW, Tchernyshyov I, Semenza GL, Dang CV. HIF-1-mediated expression of pyruvate dehydrogenase kinase: A metabolic switch required for cellular adaptation to hypoxia. *Cell Metab*. 2006;3(3):177–185.
27. Dayan F, Roux D, Brahimi-Horn MC, Pouyssegur J, Mazure NM. The oxygen sensor factor-inhibiting hypoxia-inducible factor-1α controls expression of distinct genes through the bifunctional transcriptional character of hypoxia-inducible factor-alpha. *Cancer Res*. 2006;66(7):3688–3698.
28. Frazier DP, Wilson A, Graham RM, Thompson JW, Bishopric NH, Webster KA. Acidosis regulates the stability, hydrophobicity, and activity of the BH3-only protein Bnip3. *Antioxid Redox Signal*. 2006;8(9-10):1625–1634.
29. Faraoni EY, Singh K, Chandra V, le Roux O, Dai Y, Sahin I, O'Brien BJ, Strickland LN, Li L, Vucic E, et al. CD73-dependent adenosine signaling through Adora2b drives immunosuppression in ductal pancreatic cancer. *Cancer Res*. 2023;83(7):1111–1127.
30. Rey S, Semenza GL. Hypoxia-inducible factor-1-dependent mechanisms of vascularization and vascular remodelling. *Cardiovasc Res*. 2010;86(2):236–242.
31. Gatenby RA, Gillies RJ. Why do cancers have high aerobic glycolysis? *Nat Rev Cancer*. 2004;4(11):891–899.
32. Goetze K, Walenta S, Ksiazkiewicz M, Kunz-Schughart LA, Mueller-Klieser W. Lactate enhances motility of tumor cells and inhibits monocyte migration and cytokine release. *Int J Oncol*. 2011;39(2):453–463.
33. Suzuki A, Maeda T, Baba Y, Shimamura K, Kato Y. Acidic extracellular pH promotes epithelial mesenchymal transition in Lewis lung carcinoma model. *Cancer Cell Int*. 2014;14(1):129.
34. Jiang BH, Semenza GL, Bauer C, Marti HH. Hypoxia-inducible factor 1 levels vary exponentially over a physiologically relevant range of O2 tension. *Am J Phys*. 1996;271(4):C1172–C1180.
35. Qutub AA, Popel AS. A computational model of intracellular oxygen sensing by hypoxia-inducible factor HIF1α. *J Cell Sci*. 2006;119(16):3467–3480.
36. Bagnall J, Leedale J, Taylor SE, Spiller DG, White MRH, Sharkey KJ, Bearon RN, Sée V. Tight control of hypoxia-inducible factor-α transient dynamics is essential for cell survival in hypoxia. *J Biol Chem*. 2014;289(9):5549–5564.
37. Nguyen LK, Cavadas MAS, Scholz CC, Fitzpatrick SF, Bruning U, Cummins EP, Tambuwala MM, Manresa MC, Kholodenko BN, Taylor CT, et al. A dynamic model of the hypoxia-inducible factor 1 α (HIF-1 α) network. *J Cell Sci*. 2013;126(6):1454–1463.
38. Metzen E, Berchner-Pfannschmidt U, Stengel P, Marxsen JH, Stolze I, Klinger M, Huang WQ, Wotzlaw C, Hellwig-Bürgel T, Jelkmann W, et al. Intracellular localisation of human HIF-1 alpha hydroxylases: Implications for oxygen sensing. *J Cell Sci*. 2003;116(7):1319–1326.
39. Gaete D, Rodriguez D, Watts D, Sormendi S, Chavakis T, Wielockx B. HIF-prolyl hydroxylase domain proteins (PHDs) in cancer-potential targets for anti-tumor therapy? *Cancers*. 2021;13(5):988.
40. Huang J, Zhao Q, Mooney SM, Lee FS. Sequence determinants in hypoxia-inducible factor-1α for hydroxylation by the prolyl hydroxylases PHD1, PHD2, and PHD3. *J Biol Chem*. 2002;277(42):39792–39800.
41. Gothié E, Richard DE, Berra E, Pagès G, Pouysségur J. Identification of alternative spliced variants of human hypoxia-inducible factor-1 alpha. *J Biol Chem*. 2000;275(10):6922–6927.
42. Chiang CH, Chu PY, Hou MF, Hung WC. MiR-182 promotes proliferation and invasion and elevates the HIF-1α -VEGF-A axis in breast cancer cells by targeting FBXW7. *Am J Cancer Res*. 2016;6(8):1785–1798.
43. Pereira KMA, Chaves FN, Viana TSA, Carvalho FSR, Costa FWG, Nunes Alves APN, Sousa FB. Oxygen metabolism in oral cancer: HIF and GLUTs (review). *Oncol Lett*. 2013;6(2):311–316.
44. Halestrap AP, Wilson MC. The monocarboxylate transporter family—Role and regulation. *IUBMB Life*. 2012;64(2):109–119.
45. Pouysségur J, Dayan F, Mazure NM. Hypoxia signalling in cancer and approaches to enforce tumour regression. *Nature*. 2006;441(7092):437–443.
46. Pérez de Heredia F, Wood IS, Trayhurn P. Hypoxia stimulates lactate release and modulates monocarboxylate transporter (MCT1, MCT2, and MCT4) expression in human adipocytes. *Pflugers Arch*. 2010;459(3):509–518.
47. Minchenko O, Opentanova I, Caro J. Hypoxic regulation of the 6-phosphofructo-2-kinase/fructose-2,6-bisphosphatase gene family (PFKFB-1-4) expression in vivo. *FEBS Lett*. 2003;554(3):264–270.
48. Minchenko A, Leshchinsky I, Opentanova I, Sang N, Srinivas V, Armstead V, Caro J. Hypoxia-inducible factor-1-mediated expression of the 6-phosphofructo-2-kinase/fructose-2,6-bisphosphatase-3 (PFKFB3) gene. Its possible role in the Warburg effect. *J Biol Chem*. 2002;277(8):6183–6187.
49. Alfarouk KO, Verduzco D, Rauch C, Muddathir AK, Bashir AHH, Elhassan GO, Ibrahim ME, Orozco JDP,

Cardone RA, Reshkin SJ, et al. Glycolysis, tumor metabolism, cancer growth and dissemination. A new pH-based etiopathogenic perspective and therapeutic approach to an old cancer question. *Oncoscience*. 2014;1(12):777–802.
50. Steingold JM, Hatfield SM. Targeting hypoxia-A2A adenosinergic immunosuppression of antitumor T cells during cancer immunotherapy. *Front Immunol*. 2020;11:570041.
51. Cheu JWS, Chiu DKC, Kwan KKL, Yang C, Yuen VWH, Goh CC, Chui NNQ, Shen W, Law CT, Li Q, et al. Hypoxia-inducible factor orchestrates adenosine metabolism to promote liver cancer development. *Sci Adv*. 2023;9(18):eade5111.
52. Figarella K, Kim J, Ruan W, Mills T, Eltzschig HK, Yuan X. Hypoxia-adenosine axis as therapeutic targets for acute respiratory distress syndrome. *Front Immunol*. 2024;15:1328565.
53. Strickland LN, Faraoni EY, Ruan W, Yuan X, Eltzschig HK, Bailey-Lundberg JM. The resurgence of the Adora2b receptor as an immunotherapeutic target in pancreatic cancer. *Front Immunol*. 2023;14:1163585.
54. Sweed D, Taha M, Abd Elhamed S, El Dein Mohamed AS. The prognostic role of CD73/A2AR expression and tumor immune response in periampullary carcinoma subtypes. *Asian Pac J Cancer Prev*. 2022;23(4):1239–1246.
55. Tittarelli A, Janji B, Van Moer K, Noman MZ, Chouaib S. The selective degradation of synaptic Connexin 43 protein by hypoxia-induced autophagy impairs natural killer cell mediated tumor cell killing. *J Biol Chem*. 2015;290(39):23670–23679.
56. Turner MS, Haywood GA, Andreka P, You L, Martin PE, Evans WH, Webster KA, Bishopric NH. Reversible connexin 43 dephosphorylation during hypoxia and reoxygenation is linked to cellular ATP levels. *Circ Res*. 2004;95(7):726–733.
57. Han XJ, Zhang WF, Wang Q, Li M, Zhang CB, Yang ZJ, Tan RJ, Gan LJ, Zhang LL, Lan XM, et al. HIF-1α promotes the proliferation and migration of pulmonary arterial smooth muscle cells via activation of Cx43. *J Cell Mol Med*. 2021;25:10663–10673.
58. Faigle M, Seessle J, Zug S, El Kasmi KC, Eltzschig HK. ATP release from vascular endothelia occurs across Cx43 hemichannels and is attenuated during hypoxia. *PLoS ONE*. 2008;3(7):e2801.
59. Yuan X, Lee JW, Bowser JL, Neudecker V, Sridhar S, Eltzschig HK. Targeting hypoxia signaling for perioperative organ injury. *Anesth Analg*. 2018;126(1):308–321.
60. Eckle T, Kewley EM, Brodsky KS, Tak E, Bonney S, Gobel M, Anderson D, Glover LE, Riegel AK, Colgan SP, et al. Identification of hypoxia-inducible factor HIF-1A as transcriptional regulator of the A2B adenosine receptor during acute lung injury. *J Immunol*. 2014;192(3):1249–1256.
61. Millauer B, Shawver LK, Plate KH, Risau W, Ullrich A. Glioblastoma growth inhibited in vivo by a dominant-negative Flk-1 mutant. *Nature*. 1994;367(6463):576–579.
62. Gerhardt H, Golding M, Fruttiger M, Ruhrberg C, Lundkvist A, Abramsson A, Jeltsch M, Mitchell C, Alitalo K, Shima D, et al. VEGF guides angiogenic sprouting utilizing endothelial tip cell filopodia. *J Cell Biol*. 2003;161(6):1163–1177.
63. Akwii RG, Sajib MS, Zahra FT, Mikelis CM. Role of angiopoietin-2 in vascular physiology and pathophysiology. *Cells*. 2019;8(5):471.
64. Zhang L, Li Y, Dai Y, Wang D, Wang X, Cao Y, Liu W, Tao Z. Glycolysis-related gene expression profiling serves as a novel prognosis risk predictor for human hepatocellular carcinoma. *Sci Rep*. 2021;11:18875.
65. Turner KJ, Crew JP, Wykoff CC, Watson PH, Poulsom R, Pastorek J, Ratcliffe PJ, Cranston D, Harris AL. The hypoxia-inducible genes VEGF and CA9 are differentially regulated in superficial vs invasive bladder cancer. *Br J Cancer*. 2002;86(8):1276–1282.
66. Hammond EM, Denko NC, Dorie MJ, Abraham RT, Giaccia AJ. Hypoxia links ATR and p53 through replication arrest. *Mol Cell Biol*. 2002;22(6):1834–1843.
67. Chen J, Yue H, Ouyang Q. Correlation between oncogenic mutations and parameter sensitivity of the apoptosis pathway model. *PLoS Comput Biol*. 2014;10(1):e1003451.
68. Ruan K, Song G, Ouyang G. Role of hypoxia in the hallmarks of human cancer. *J Cell Biochem*. 2009;107(6):1053–1062.
69. Ma Y, Liang AJ, Fan YP, Huang YR, Zhao XM, Sun Y, Chen XF. Dysregulation and functional roles of miR-183-96-182 cluster in cancer cell proliferation, invasion and metastasis. *Oncotarget*. 2016;7(27):42805–42825.
70. Kouri FM, Hurley LA, Daniel WL, Day ES, Hua Y, Hao L, Peng CY, Merkel TJ, Queisser MA, Ritner C, et al. miR-182 integrates apoptosis, growth, and differentiation programs in glioblastoma. *Genes Dev*. 2015;29(7):732–745.
71. Li Y, Zhang H, Li Y, Zhao C, Fan Y, Liu J, Li X, Liu H, Chen J. MiR-182 inhibits the epithelial to mesenchymal transition and metastasis of lung cancer cells by targeting the met gene. *Mol Carcinog*. 2018;57(1):125–136.
72. Petrella BL, Lohi J, Brinckerhoff CE. Identification of membrane type-1 matrix metalloproteinase as a target of hypoxia-inducible factor-2α in von Hippel–Lindau renal cell carcinoma. *Oncogene*. 2005;24(6):1043–1052.
73. Williams AL, Khadka VS, Anagaran MCT, Lee K, Avelar A, Deng Y, Shohet RV. miR-125 family regulates XIRP1 and FIH in response to myocardial infarction. *Physiol Genomics*. 2020;52(2):358–368.
74. Kelly TJ, Souza AL, Clish CB, Puigserver P. A hypoxia-induced positive feedback loop promotes hypoxia-inducible factor 1alpha stability through miR-210 suppression of glycerol-3-phosphate dehydrogenase 1-like. *Mol Cell Biol*. 2011;31(13):2696–2706.
75. Neudecker V, Brodsky KS, Kreth S, Ginde AA, Eltzschig HK. Emerging roles for microRNAs in perioperative medicine. *Anesthesiology*. 2016;124(2):489–506.
76. Ju C, Wang M, Tak E, Kim B, Emontzpohl C, Yang Y, Yuan X, Kutay H, Liang Y, Hall DR, et al. Hypoxia-inducible factor–1α –dependent induction of miR122 enhances hepatic ischemia tolerance. *J Clin Invest*. 2021;131(7):e140300.
77. Czopik AK, McNamee EN, Vaughn V, Huang X, Bang IH, Clark T, Wang Y, Ruan W, Nguyen T, Masterson JC, et al. HIF-2α-dependent induction of miR-29a restrains T_H1 activity during T cell dependent colitis. *Nat Commun*. 2024;15:8042.
78. Vande Velde C, Cizeau J, Dubik D, Alimonti J, Brown T, Israels S, Hakem R, Greenberg AH. BNIP3 and genetic control of necrosis-like cell death through the mitochondrial permeability transition pore. *Mol Cell Biol*. 2000;20(15):5454–5468.
79. Burton TR, Gibson SB. The role of Bcl-2 family member BNIP3 in cell death and disease: NIPping at the heels of cell death. *Cell Death Differ*. 2009;16(4):515–523.

80. Hendgen-Cotta UB, Esfeld S, Rudi K, Miinalainen I, Klare J, Rassaf T. Cytosolic bnip3 dimer interacts with mitochondrial bax forming heterodimers in the mitochondrial outer membrane under basal conditions. *Int J Mol Sci*. 2017;18(4):687.
81. Bellot G, Garcia-Medina R, Gounon P, Chiche J, Roux D, Pouysségur J, Mazure NM. Hypoxia-induced autophagy is mediated through hypoxia-inducible factor induction of BNIP3 and BNIP3L via their BH3 domains. *Mol Cell Biol*. 2009;29(10):2570–2581.
82. Bredholt G, Mannelqvist M, Stefansson IM, Birkeland E, Bø TH, Øyan AM, Trovik J, Kalland KH, Jonassen I, Salvesen HB, et al. Tumor necrosis is an important hallmark of aggressive endometrial cancer and associates with hypoxia, angiogenesis and inflammation responses. *Oncotarget*. 2015;6(37):39676–39691.
83. Papale M, Buccarelli M, Mollinari C, Russo MA, Pallini R, Ricci-Vitiani L, Tafani M. Hypoxia, inflammation and necrosis as determinants of glioblastoma cancer stem cells progression. *Int J Mol Sci*. 2020;21(8):2660.
84. Karsch-Bluman A, Feiglin A, Arbib E, Stern T, Shoval H, Schwob O, Berger M, Benny O. Tissue necrosis and its role in cancer progression. *Oncogene*. 2019;38(11):1920–1935.
85. Yee PP, Li W. Tumor necrosis: A synergistic consequence of metabolic stress and inflammation. *BioEssays*. 2021;43(7):e2100029.
86. DiGiacomo JW, Gilkes DM. Tumor hypoxia as an enhancer of inflammation-mediated metastasis: Emerging therapeutic strategies. *Target Oncol*. 2018;13(2):157–173.
87. Zhang X, Chen L. The recent progress of the mechanism and regulation of tumor necrosis in colorectal cancer. *J Cancer Res Clin Oncol*. 2016;142(2):453–463.
88. Liu Q, Palmgren VAC, Danen EH, Le Dévédec SE. Acute vs. chronic vs. intermittent hypoxia in breast cancer: A review on its application in in vitro research. *Mol Biol Rep*. 2022;49(11):10961–10973.
89. Feng X, Liu X, Zhang W, Xiao W. p53 directly suppresses BNIP3 expression to protect against hypoxia-induced cell death. *EMBO J*. 2011;30(16):3397–3415.
90. Schmid T, Zhou J, Köhl R, Brüne B. p300 relieves p53-evoked transcriptional repression of hypoxia-inducible factor-1 (HIF-1). *Biochem J*. 2004;380(Pt 1):289–295.
91. Joshi S, Singh AR, Durden DL. MDM2 regulates hypoxic hypoxia-inducible factor 1 α stability in an E3 ligase, proteasome, and PTEN-phosphatidylinositol 3-kinase-AKT dependent manner. *J Biol Chem*. 2014;289(33):22785–22797.
92. Yu L, Wu M, Zhu G, Xu Y. Emerging roles of the tumor suppressor p53 in metabolism. *Front Cell Dev Biol*. 2022;9:762742.
93. Wang P, Guan D, Zhang XP, Liu F, Wang W. Modeling the regulation of p53 activation by HIF-1 upon hypoxia. *FEBS Lett*. 2019;593(18):2596–2611.
94. Albadari N, Deng S, Li W. The transcriptional factors HIF-1 and HIF-2 and their novel inhibitors in cancer therapy. *Expert Opin Drug Discov*. 2019;14(7):667–682.
95. D'Ignazio L, Bandarra D, Rocha S. NF-κB and HIF crosstalk in immune responses. *FEBS J*. 2015;283(3):413–424.
96. Rius J, Guma M, Schachtrup C, Akassoglou K, Zinkernagel AS, Nizet V, Johnson RS, Haddad GG, Karin M. NF-κB links innate immunity to the hypoxic response through transcriptional regulation of HIF-1α. *Nature*. 2008;453(7196):807–809.
97. Thattai M, van Oudenaarden A. Intrinsic noise in gene regulatory networks. *Proc Natl Acad Sci USA*. 2001;98(15):8614–8619.
98. Kang X, Wang J, Li C. Exposing the underlying relationship of cancer metastasis to metabolism and epithelial-mesenchymal transitions. *iScience*. 2019;21:754–772.
99. Liang Y, Ruan W, Jiang Y, Smalling R, Yuan X, Eltzschig HK. Interplay of hypoxia-inducible factors and oxygen therapy in cardiovascular medicine. *Nat Rev Cardiol*. 2023;20(11):723–737.
100. Provenzano R, Besarab A, Wright S, Dua S, Zeig S, Nguyen P, Poole L, Saikali KG, Saha G, Hemmerich S, et al. Roxadustat (FG-4592) versus epoetin alfa for anemia in patients receiving maintenance hemodialysis: A phase 2, randomized, 6- to 19-week, open-label, active-comparator, dose-ranging, safety and exploratory efficacy study. *Am J Kidney Dis*. 2016;67(6):912–924.
101. Habas ES, Al Adab A, Arryes M, Alfitori G, Farfar K, Habas AM, Akbar RA, Rayani A, Habas E, Elzouki A. Anemia and hypoxia impact on chronic kidney disease onset and progression: Review and updates. *Cureus*. 2023;15(10):e46737.
102. Semenza GL. Pharmacologic targeting of hypoxia-inducible factors. *Annu Rev Pharmacol Toxicol*. 2019;59:379–403.
103. Bosch-Marce M, Okuyama H, Wesley JB, Sarkar K, Kimura H, Liu YV, Zhang H, Strazza M, Rey S, Savino L, et al. Effects of aging and hypoxia-inducible factor-1 activity on angiogenic cell mobilization and recovery of perfusion after limb ischemia. *Circ Res*. 2007;101(12):1310–1318.